INSTITUTE OF PHYSICS PUBLISHING JOURNAL OF PHYSICS D: APPLIED PHYSICS

J. Phys. D: Appl. Phys. **39** (2006) R125–R150 doi:10.1088/0022-3727/39/7/R01

TOPICAL REVIEW

Ferromagnetic manganites: spin-polarized conduction versus competing interactions

Kathrin Dörr

IFW Dresden, Institute for Metallic Materials, Postfach 270116, D-01171 Dresden, Germany

E-mail: k.doerr@ifw-dresden.de

Received 31 October 2005
Published 17 March 2006
Online at stacks.iop.org/JPhysD/39/R125

Abstract

Manganese oxides $(R,A)MnO_3$ (R = La, Y, Bi or rare earth metal, A = non-trivalent doping element) have been one focus of research for two outstanding properties: (i) conduction electrons (if any) are highly spin-polarized and (ii) competing interactions of several electronic and lattice degrees of freedom lead to extremely rich phase diagrams and complex physics. A better understanding of the latter might result in future technologies using manganites in spin-electronic devices. This review attempts to systematically outline in a phenomenological approach some fundamentals and key experiments on ferromagnetic manganites, partially with respect to thin film structures. Macroscopic magnetic properties (of ferromagnets and glassy manganites) and intrinsic electron transport are described. Preparation and basic properties of thin films, followed by experiments on spin-polarized tunnelling are reviewed. Finally, multiferroic heteroepitaxial film systems of manganites and ferroelectric titanates are addressed, which are promising candidates for significant magnetoelectric phenomena at ambient temperatures.

(Some figures in this article are in colour only in the electronic version)

1. Introduction

Electronic properties of solids are vitally important if one thinks of applications in microelectronics, magnetic data storage, communication technologies and other fields. Sometimes, it seems possible to postpone the step of fundamental understanding when starting the application of a new material. Nevertheless, the lasting success and discovery of principally new solutions is based on it.

Electronic properties of 3d transition metal (TM) (e.g. Ti, Mn, Fe, Cr, Co, Cu) oxides are much less understood than those of elemental metals, oxide ionic insulators or lightly doped classical semiconductors. One reason for this situation is the strong correlation of 'more or less' localized 3d electrons that, on the one hand, is responsible for the rich physics of 3d TM compounds but has made theoretical modelling very difficult. Unforeseen phenomena have been discovered just for some oxides of 3d metals in the last two decades of the 20th century: high-temperature superconductivity in cuprates, colossal magnetoresistance (CMR) in manganites, high spin polarization of conduction electrons in CrO_2, Fe_3O_4 and manganites, ferromagnetism in dilute magnetic semiconductors (DMS) (titanates, ZnO) and low-dimensional behaviour in cuprates. All these phenomena are based on the strong interrelation between the magnetic and electronic (charge carriers, orbitals) degrees of freedom. Additionally, the crystal lattice couples to electronic modes.

Early work on doped manganites $(La,A)MnO_3$ (A = Sr; Ca; Pb; Ba) started before 1950, when Jonker, van Santen and Volger [1, 2] from Philips, Eindhoven, investigated sintered ceramics in a search for insulating ferromagnets for transformers. Instead, they discovered ferromagnetism

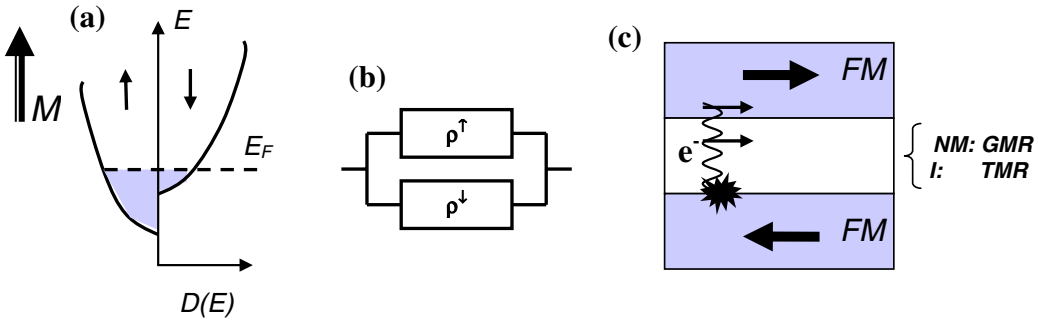

Figure 1. (*a*) Schematic density of electronic states (DOS) versus energy of a conducting ferromagnet. The subbands with electron spin parallel or antiparallel to the spontaneous magnetization (M) are split, resulting in different DOS at the Fermi level E_F. (*b*) Two-channel model of electronic conduction, with spin up and spin down electrons in independent channels. (*c*) Trilayer junction comprising two ferromagnetic layers and a non-magnetic interlayer which is a metal in GMR junctions and an insulator in a tunnel junction. The small arrows indicate the spin of a majority electron moving through the layer stack and being strongly scattered (in case of GMR) at the interface to the electrode magnetized oppositely.

associated with metallic conduction and large negative magnetoresistance (MR) [3]. This observation triggered the development of the double exchange concept by Zener [4] where ferromagnetic interaction of localized 3d magnetic moments is mediated by spin-polarized conduction electrons. Another important theoretical concept developed in this context is the Jahn–Teller (JT) polaron (e.g. [5, 6]), the lattice distortion of oxygen octahedra around Mn^{3+} ions that lifts the degeneracy of 3d e_g electronic states. A strong revival of manganite research occured around 1995, since manganite were at an overlap of three expanding research areas: similar in chemistry and certain electronic properties to cuprate superconductors, manganites could be prepared by emerging thin film preparation techniques. Furthermore, they showed large MR [7] and spin polarization, making them potential candidates for an arising spintronics technology. However, it was realized that the way into technology is not as straightforward for manganites as it was, for example, for giant magnetoresistance (GMR) in metallic multilayers. GMR was discovered in 1988 [8, 9] and is currently applied in magnetic sensors including read heads of hard disc drives. On the other hand, the physics of manganites is only partially understood and, even now, new parameters and phenomena are being discovered.

This review attempts to give a phenomenological introduction to the physics of ferromagnetic manganites and to assemble a consistent picture of some key experiments on magnetic and electrical behaviour. Section 2 is devoted to fundamental microscopic mechanisms. Section 3 is concerned with magnetic order phenomena including glassy states. Section 4 describes the intrinsic electrical behaviour of ferromagnetic manganites and current understanding of the origin of CMR. Thin film preparation, microstructure of films and multilayers and some magnetic/electric properties of films deviating from bulk are adressed in section 5. Examples for spin-polarized tunnelling in trilayer films and at grain boundaries (GB) are discussed in section 6. Finally, Section 7 is devoted to epitaxial systems of manganites with ferroelectric titanates. These show both, ferroelectric and ferromagnetic polarization, and may open up new ways for electric control of magnetic properties.

2. Fundamentals

2.1. Spin-polarized electron conduction

Conduction electrons in ferromagnetic metals can be considered to reside in two 'conduction channels', with the electron spin being either parallel ('spin-up') or antiparallel ('spin-down') to the magnetization vector. There is no intermixing between the channels if no spin-flip scattering occurs, the conductivities of both channels just add up to the total conductivity. The electronic density of states (DOS) is split into a spin-up and a spin-down sub-band (figure 1), with a relative shift of the spin-down band towards higher energy. The difference of the DOS in the two channels ($n_\uparrow$; $n_\downarrow$) at the Fermi energy (E_F) produces the *spin polarization* of conduction electrons, $P = (n_\uparrow - n_\downarrow) / (n_\uparrow + n_\downarrow)$. Note that the spin polarization of a current flowing in a material might differ from P due to different velocities of $n_\uparrow$ and $n_\downarrow$ electrons; this is the so-called *transport spin polarization*.

Some magnetic materials appear to have no states at E_F in one of the subbands, i.e. charge carriers have only one spin direction. They are called *half-metals*. Half-metals are particularly interesting for spintronics as a source of fully spin-polarized electrons. Sometimes, half-metals are predicted by band structure calculations. Any experimental verification of 'complete' spin polarization is naturally difficult. Large spin-polarization can be evidenced, e.g. by spin-resolved photoelectron spectroscopy, Andreev reflection or large tunnel MR (6.2).

The two-channel model provides a simple explanation for the best-known example of spin-polarized conduction, the GMR. In a spin valve structure (figure 1), spin-polarized electrons travel through a non-magnetic metal interlayer separating two ferromagnetic (FM) layers. Essentially, spin-dependent scattering occurs only at the interfaces. For parallel magnetization directions of both FM layers, spin-up electrons can pass with little scattering at both interfaces; thus, resistance of the layer stack is lower than that for antiparallel magnetization directions. If the interlayer is replaced by an insulator with the thickness of a few nanometres, a magnetic tunnel junction is obtained, which is the other spintronics device that has already achieved commercial relevance (as magnetic random access memory, MRAM). According to

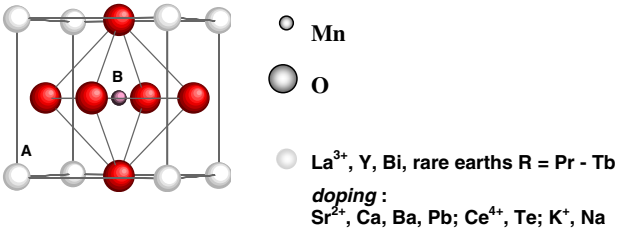

Figure 2. Pseudocubic unit cell of the perovskite-like lattice of doped $LaMnO_3$. Mn on the lattice B site is centred in an oxygen octahedron. La on lattice A site can be replaced or partially substituted by several metal ions of appropriate ionic radius (see text). Non-trivalent metals act as dopants.

Julliere's model, electrons tunnel through an insulator with a probability proportional to the product of the occupied DOS in the start electrode and the empty DOS (at same energy and spin) in the final electrode [10]. In the case of a half-metal, tunnelling is forbidden for antiparallel orientation of the magnetization vectors of FM layers. Alignment of magnetization by a modest magnetic field produces a huge resistance drop or *tunnelling MR* (TMR).

There are more devices utilizing spin polarization of charge carriers and a magnetic field for the control of electrical resistance or current. Examples are the spin valve transistor [11], the magnetic tunnel transistor [12] and spin injection devices [13].

2.2. Oxides with high spin polarization

The property of high spin polarization is restricted to a very low fraction of all ferromagnetic conductors. Elemental ferromagnetic 3d metals have $P < 50\%$. Solid Mn is an antiferromagnetic (AFM) metal. Interestingly, several Mn compounds exhibit high (transport) spin polarization: NiMnSb [14], $La_{0.7}Sr_{0.3}MnO_3$ [15], $Tl_2Mn_2O_7$ [16], Mn doped semiconductors (e.g. (Ga,Mn)As) [17]. Oxides of TMs have rather narrow conduction bands (of the order of ∼1 eV), comparable to the Stoner splitting energy of spin-up and spin-down subbands (figure 1). Thus, the splitting may produce a *half-metal*-like DOS. Well-known examples are CrO_2, $La_{0.7}Sr_{0.3}MnO_3$, the double perovskite Sr_2FeMoO_6 and the ferrimagnet Fe_3O_4 with activated polaronic conduction; all of them reviewed by Ziese [18].

2.3. Rare earth manganites

$LaMnO_3$ is the parent compound of rare earth manganites, an AFM insulator. The lattice structure of manganites is perovskite-like and nearly cubic (figure 2). Rhombohedral, orthorhombic or other lattice distortions result from the tilting and stretching of oxygen octahedra around Mn ions. These distortions appear for structural (mismatch of ionic radii) and electronic (JT effect of Mn^{3+}) reasons. Chemical substitution is possible at all lattice sites. La^{3+} can be replaced by rare earth elements, Y and Bi, as well as by divalent (Sr, Ca, Ba, Pb), tetravalent (Ce, Te, Sn) and monovalent (K, Na) elements. Non-trivalent substitutions act as dopants: they induce a mixed Mn valence and, thereby, charge carriers. Mn can be replaced by most 3d (e.g. Ti, Ga) and some 4d (e.g. Ru) elements; this commonly results in a suppressed FM order (3.2). The oxygen

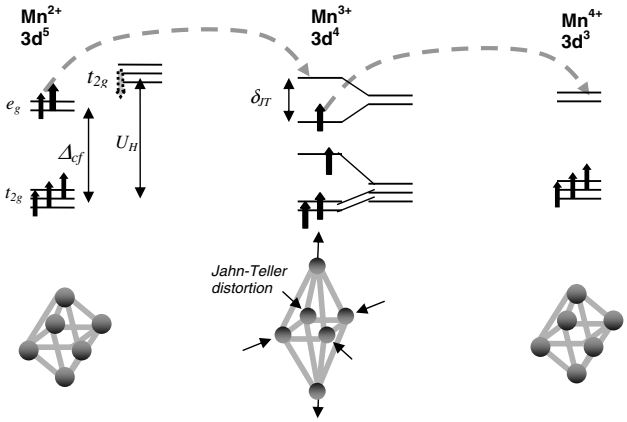

Figure 3. Single ion scheme of 3d electronic states in Mn^{2+}, Mn^{3+} and Mn^{4+} ions in perovskite manganites. Abbreviations denote Δ_{cf} octahedral crystal field splitting, U_H Hund's rule onsite coupling energy, δ_{JT} Jahn-Teller splitting energy resulting from distortion of the oxygen octahedron (as sketched below). Large dashed arrows indicate spin-conservative electron transfer between Mn ions which proceeds via intermediate O 2p orbitals.

content can be enhanced or reduced, the first meaning metal vacancies and the latter oxygen vacancies in the lattice, since no interstitial sites are available in the lattice. The Goldschmidt tolerance factor [19] calculated from ionic radii in a general ABO_3 perovskite structure (figure 2)

$$t = \frac{r(\mathrm{A}) + r(\mathrm{O})}{\sqrt{2}[r(\mathrm{B}) + r(\mathrm{O})]}, \qquad (1)$$

with site B inside the oxygen octahedron, accounts for which elements fit into the Mn perovskite lattice and at what lattice site. $r(\mathrm{A})$ and $r(\mathrm{B})$ denote the average ionic radii at the A and B sites and $r(\mathrm{O})$ is the radius of the O^{2-} ion. $t = 1$ characterizes the cubic structure, and the distorted perovskite-like structures exist approximately in the range of $0.89 < t < 1.02$. Most manganites represent the case $t < 1$.

2.4. Electronic structure and magnetic exchange

The electronic structure of manganites is more complicated than what can be described in a simple ionic scheme (figure 3); nevertheless this approach is useful in outlining the most important interactions. Mn^{2+}, Mn^{3+} and Mn^{4+} valence states found in manganites have 5, 4 or 3 electrons in the 3d level, all with parallel spins according to Hund's first rule. Hund's rule coupling energy U_{H} is particularly large for Mn, about 2 eV [20]. The three lower lying t_{2g} levels resulting from the crystal field splitting in the octahedral oxygen environment form a core magnetic moment of 3 μ_{B}, since t_{2g} electrons are always localized in manganites. The remaining electrons (one for Mn^{3+}, two for Mn^{2+}) occupy the e_g level and are delocalized or localized depending on the case. Delocalization via O 2p orbitals is most favoured for Mn–O–Mn bond angles of 180° (as present in the cubic structure).

Due to their parallel coupling to Mn core moments, electrons moving with conserved spin mediate a ferromagnetic exchange interaction. Zener introduced the concept of ferromagnetic *double exchange* [4] for manganites, assuming two simultaneous electron transfers: one electron from Mn^{3+} to

a neighbouring O 2p orbital and a second electron from this O 2p orbital to an adjacent Mn^{4+} ion. The final and original states of this process are degenerate and, thus, coexist and couple the two Mn moments ferromagnetically. More generally, double exchange means a magnetic interaction mediated by itinerant spin-polarized d electrons which couple according to Hund's rule to the localized magnetic moments [21]. Itinerancy of electrons is energetically favourable for kinetic energy gain. It is useful to note that this model ignores the role of oxygen. This is possibly oversimplified. For instance, an electron hole might reside at an oxygen site between two Mn^{3+} ions or even be distributed in non-integer fractions in a Mn–O–Mn pair [22, 23].

In a semiclassical treatment, double exchange leads to a specific dependence of electron transfer between Mn ions on the angle Θ between their magnetic moments: $t = t_0 \cos(\Theta/2)$ [24]. The transfer probability varies from 1 for $\Theta = 0$ to zero for $\Theta = 180^\circ$. This simple relation illustrates the origin of a large MR observable in double exchange ferromagnets: if a magnetic field is strong enough to align the magnetic core moments, resistance would drop drastically.

Apart from the double exchange, superexchange interactions of both, Mn t_{2g} and e_g orbitals via O 2p orbitals are present. Superexchange interactions have been analysed in detail by Goodenough [25] (also see the Goodenough–Kanamori rules [26]). Superexchange can be ferromagnetic or AFM, as in the case of $Mn^{3+}e_g$–O–$Mn^{4+}e_g$ where it depends on the orientation of the $Mn^{3+}e_g$ orbital. One prominent example is $LaMnO_3$ with only Mn^{3+} ions present and an A-type AFM structure: ferromagnetic Mn^{3+}–O–Mn^{3+} superexchange dominates within parallel lattice planes, with neighbouring planes coupled antiferromagnetically. The A-type AFM structure consists of ferromagnetically aligned magnetic moments within cubic (001) planes and alternating direction of moments in adjacent planes. Therefore, the orbital degree of freedom is essential for manganite physics.

The strong *JT effect* of Mn^{3+} is another important microscopic mechanism of manganites physics (figure 3) [27]. It is the source of strong electron–phonon coupling. Deformation of the oxygen octahedron around Mn^{3+} ions lifts the degeneracy of e_g levels and reduces the electronic energy for the single e_g occupation. (It also reduces the total energy.) Elongation of the O octahedron favours occupation of the e_g $3z^2 - r^2$ orbital, while compression favours the e_g $x^2 - y^2$ orbital. The JT splitting energy is about $\Delta_{JT} = 1$–1.5 eV [28]. Moving e_g electrons may form lattice polarons arising from the JT distortions, and 'trapping' (localization) of charge carriers by elastic distortions is possible. For metallic manganites, the JT distortions are dynamic, resulting in an average distortion of all O_6 octahedra.

Most known manganites have an average Mn charge between +3 and +4, such as the prototype compound $La_{2/3}Sr_{1/3}MnO_3$ with hole-type charge carriers. $CaMnO_3$ is an example of a pure Mn^{4+} compound, and small substitution of, e.g. La^{3+} into $CaMnO_3$ creates electron-type charge carriers. On the contrary, few manganites with Mn charge between +2 and +3 have been studied. Ce-, Te- and Sn-doped $LaMnO_3$ nominally belong to this group of electron-doped $LaMnO_3$, although the actual doping also depends on oxygen stoichiometry. For electron-doped $LaMnO_3$, an interesting question arose about the spin polarization [29]: since Mn^{2+} has two e_g electrons, the second one could reside in a $t_{2g}^{\downarrow}$ (spin-down) state, if U_H is as small as $U_H < \Delta_{CF} + 0.5\delta_{JT}$ (figure 3), with the crystal field splitting energy Δ_{CF}.

For aspects of band structure, see, for instance, the review articles of Gor'kov and Kresin and Dagotto *et al* [21, 30].

2.5. Electron lattice coupling

The size mismatch of ions substituted into the perovskite lattice (the so-called *chemical pressure effect*) causes a reduction in the Mn–O–Mn bond angles from 180° down to 160° and below. Thereby, the conduction band width (W) is reduced due to a smaller orbital overlap. Bond length changes are another consequence of the varied ionic radii, additionally influencing W. Most manganites have a tolerance factor $t < 1$, i.e. the ions on the La site are too small. With an increasing r(A), one observes both, increasing average bond angle (enhanced W) and bond length (reduced W) [31]. Hence, the ferromagnetic Curie temperature T_C of $R_{0.7}A_{0.3}MnO_3$ increases with r(A) but drops when the effect of the increasing bond length starts to dominate (for A = Pb; Ba) [31].

The other source of electron lattice coupling is the JT effect (2.4) [27]. JT deformations of O_6 octahedra can be long-range ordered (*orbital order*, OO), as found in $LaMnO_3$. Two or three distinct Mn–O bond lengths are detectable, and the crystal structure is of a lower symmetry (orthorhombic, monoclinic). In doped manganites, superstructures of localized charge carriers (*charge order*, CO) usually accompany the orbital order. CO/OO has been observed for numerous insulating manganites. Charge ordering naturally competes with the ferromagnetic double exchange, since it tends to localize charge carriers.

Electron–lattice coupling is reflected in several macroscopic properties, for instance, in strong lattice contraction upon cooling through T_C [32], large or anomalous magnetostriction of some manganites [32], associated structural and magnetic phase transitions and strong dependence of T_C on epitaxial strain in films (5.3).

2.6. Magnetic and electronic phase diagrams

In sections 2.3–2.5, the essential contributions to electronic energy in manganites have been outlined. These are summarized as follows: (i) kinetic energy of e_g electrons, (ii) the Hund on-site magnetic coupling between e_g and t_{2g} electron spins, (iii) coupling of e_g electrons and elastic distortions of MnO_6 octahedra (JT effect), (iv) the crystal field splitting energy in octahedral coordination, (v) the Heisenberg magnetic coupling between the nearest-neighbour localized electron spins and (vi) the Coulomb interaction among e_g electrons [21]. The dominance of one or the other mechanism results in various ground states. The ground state of $R_{1-x}A_xMnO_3$ depends on (i) the number of doped charge carriers x, (ii) the average ionic radii on La and Mn lattice sites and (iii) the scatter of ionic radii on La site measured by a *disorder parameter* σ according to the standard deviation of ionic radii [33]. Ground states observed for manganites include ferromagnetic metals (frequent), AFM insulators (many), ferromagnetic insulators (less frequent), AFM metals (rare),

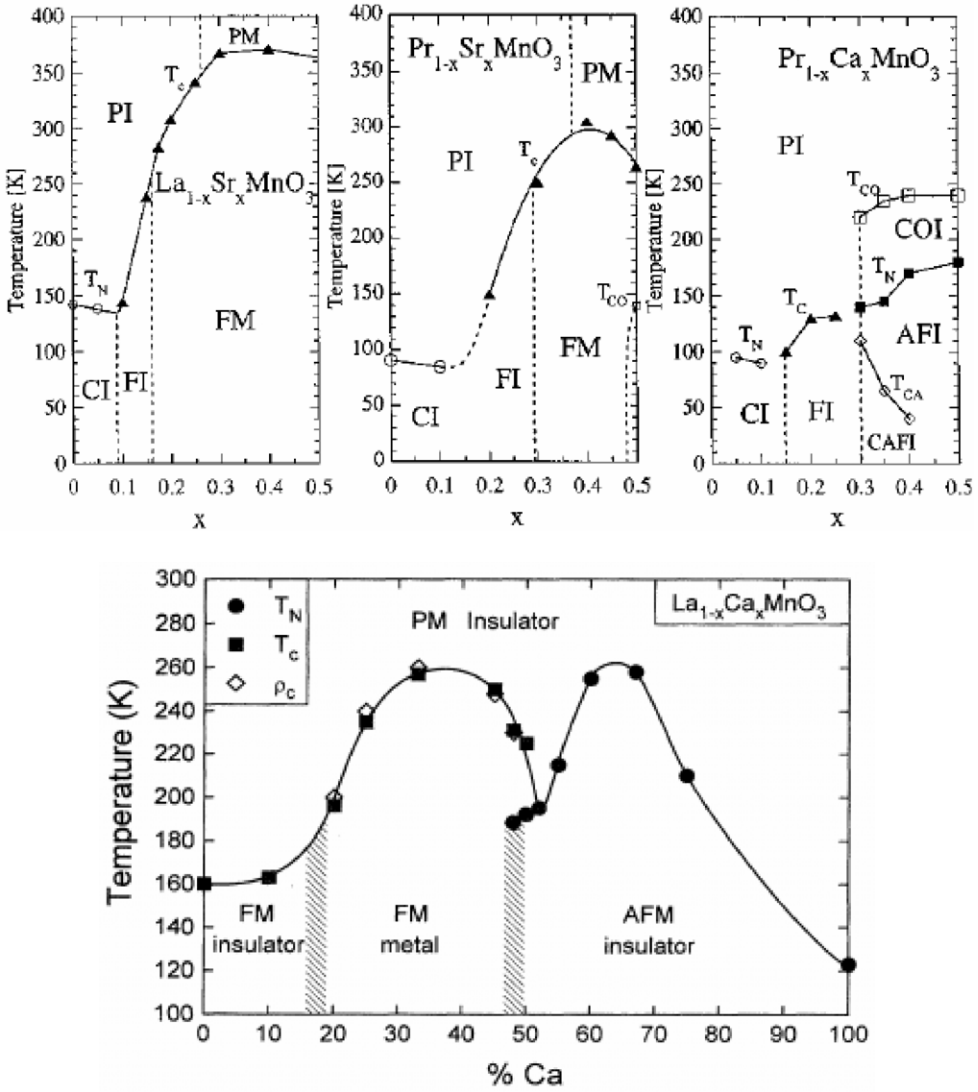

Figure 4. Magnetic and electronic phase diagram versus doping x for $La_{1-x}Sr_xMnO_3$ (large band width), $Pr_{1-x}Sr_xMnO_3$ (medium band width), $Pr_{1-x}Ca_xMnO_3$ (low band width) (all adapted with permission from [51], ©1996 AIP) and for $La_{1-x}Ca_xMnO_3$ (medium band width) (reprinted with permission from [194], ©1995 APS). Abbreviations: F—ferromagnetic, P—paramagnetic, AF—antiferromagnetic, C—canted magnetic structure, T_C—ferromagnetic Curie temperature, T_N - Néel temperature, M—metal, I—insulator and CO—charge ordered phase. Note that the FM phase region is reduced with decreasing band width. CO also exists in the low doped FI / CI region (not indicated). Regions of phase coexistence not shown (see text).

glassy insulators, more complex canted magnetic structures and mixed-phase states (see below). Almost all metallic manganites are ferromagnetic, since electron transfer enhances the double exchange. (Note that a compound is called a *metal* if its resistance grows with rising temperature, irrespective of the value of resistivity. If the resistance decreases with rising temperature, both terms *insulator* and *semiconductor* are applied without clear distinction in research on manganites.)

Phase diagrams in dependence on temperature and doping level x can be illustrated by three prominent examples: $La_{1-x}Sr_xMnO_3$, $La_{1-x}Ca_xMnO_3$ and $Pr_{1-x}Ca_xMnO_3$ (figure 4). The ionic radius r(A) reduces from La–Sr system to Pr–Ca system, leading to increasing distortions of the lattice and suppression of electron transfer. General features of the phase diagrams are the appearance of a metallic ferromagnetic (FMM) phase near $x = 0.33$, which is more extended for La–Sr compounds and completely absent for Pr–Ca compounds (where it can be induced by application of large magnetic or electric fields). This phase is interesting for applications in spintronics since it shows high spin polarization of charge carriers. Near $x \sim 0.5$, the ground state changes to antiferromagnetic insulating (AFI) and charge ordered (CO). The same is true for low doping. Various AF structures are realized depending on x: A, CE, C and G type [34]. At high temperatures, a paramagnetic (PM) and almost always insulating phase is found.

Between these three fundamental states (FMM, AFI–CO, PM) there are regions of more complex character. Originally, spin-canted magnetic structures have been proposed to exist between the FMM and AFI phase regions, in particular for low doping [35]. Recent theoretical models indicate the coexistence of two phases with different electron

densities (*electronic phase separation*) or different structural distortions [21, 36]. Experimental evidence for mixed-phase states has been collected in many ways although unambiguous interpretation is still difficult. Exclusion of nano-scale *chemical inhomogeneity* is naturally complicated. Surprisingly, the observed length scale of different phases for phase-separated manganites varies from 1 nm to nearly 1 μm. The large extension excludes different electronic density of the phases for reasons of electrostatic energy. Nuclear magnetic resonance (NMR) studies gave evidence of Mn ions with different nuclear relaxation times, attributed to the coexistence of ionic Mn^{3+}, Mn^{4+} and Mn involved in the itinerant e_g electron transfer [37, 38]. Scanning tunnelling microscopy (STM) [39–41] as a powerful surface-characterizing method detected strong spatial variations of surface conductivity in a wide temperature range, which change under the magnetic field and, moreover, can be related to cooperative shifts in atomic positions (CO in insulating regions) [41]. Transmission electron microscopy (TEM) was employed to distinguish between sample regions with CO superstructures and those without [42]. Electron holography showed the closed flux lines of the isolated FM regions [43, 44]. Clear evidence of the presence of metallic filaments in an insulating matrix is known for $Pr_{1-x}Ca_xMnO_3$ for $x \sim 0.3$ [45], where conduction paths are directly imaged. Huge random telegraph noise (RTN) of electrical resistance observed in thin films and crystals has been attributed to dynamic fluctuations of sample regions between two phases of different conductivities [46–48]. Recently, polarized small angle neutron measurements [49,50] were interpreted to show a sheet-like distribution of two phases of few nanometres width (named a 'red cabbage' structure).

If an insulating compound is near a FMM–AFI phase boundary, the metallic state may be induced by external conditions such as large magnetic [51] or electric fields [52], light [45] or x-ray irradiation [53], hydrostatic pressure [54] and strain in films [55]. When metallic regions percolate, a resistance reduction by more than six orders of magnitude is possible.

Unfortunately with respect to applications, the $T_C \sim 370$ K of $La_{0.7}Sr_{0.3}MnO_3$ is the largest known FM ordering temperature. CO can appear at temperatures as large as 525 K in $Bi_{1-x}Sr_xMnO_3$ [56].

3. Magnetic properties

3.1. Ferromagnetic phases

3.1.1. Critical behaviour near T_C. Double exchange interaction as the predominant source of ferromagnetism in manganites is based on electron transfer between Mn core spins. This triggers the question about the long-range or short-range nature of ferromagnetic ordering. Can it be described by a three-dimensional short-range (mean field, Heisenberg or Ising) coupling model? Next, some paramagnetic–ferromagnetic (PM–FM) transitions are accompanied by structural changes; one might expect such transitions to be of the first order. The order of the PM–FM transition in manganites is a second question answered only for a few compounds so far. These questions can be answered by an examination of the critical behaviour of manganites. In recent years, data on the critical behaviour at PM–FM transitions have been collected for several manganites (some listed in [57]). Most investigated FM compounds exhibit a second order transition at T_C, with critical parameters between those of the Heisenberg 3D and the mean-field models. A first order transition is known for $La_{0.7}Ca_{0.3}MnO_3$ and $La_{0.6}Y_{0.07}Ca_{0.33}MnO_3$. Tricritical points (characteristic for the crossover from first to second order behaviour) have been observed for $La_{0.6}Ca_{0.4}MnO_3$ [58] and $La_{0.67}(Ca_{0.85}Sr_{0.15})_{0.33}MnO_3$. The Ca doped system shows orthorhombic lattice symmetry and a pronounced cooperative JT effect. The lattice changes from orthorhombic to rhombohedral symmetry (without long-range ordered JT effect) for partial Sr substitution in $La_{0.67}(Ca_{1-z}Sr_z)_{0.33}MnO_3$, simultaneously with the crossover to second order type transition [59]. This experiment supports the hypothesis that first order transitions might appear in compounds with a strong cooperative JT effect. Strong lattice effects appear for the lower ionic radius r(A) and are, thus, related to the lower T_C values. However, there are low-T_C manganites such as $Nd_{0.6}Pb_{0.4}MnO_3$ with a continuous (i.e. second order) transition [57]. Since disorder at the La site is rather large for the Nd–Pb system, it seems to hinder the appearance of a first order transition. Another effect of disorder is the so-called 'rounding' of a discontinuous transition, i.e. a first order transition changes to the second order after disorder is introduced. For example, $La_{0.7}Ca_{0.3}Mn_{0.9}Ga_{0.1}O_3$ with 10% of Ga^{3+} ions in the Mn lattice has a clear second order transition [60].

The importance of disorder for the type of phase transition was emphasized, for instance, by Salamon *et al* [61] who pointed out similarities of the PM state of $La_{0.7}Ca_{0.3}MnO_3$ with a *Griffiths phase*. In a Griffiths phase, disorder (e.g. randomly broken bonds) suppresses the magnetic transition temperature from a value for the disorder-free system to a lower value. Magnetic clusters exist in the intermediate temperature range of the Griffiths phase.

Ferromagnetism is not always associated with macroscopic metallic conductivity in manganites. Three types of insulating FM manganites are known to the author: (i) ferromagnetic-metallic clusters in an insulating matrix, the phase-separation case, (ii) local double-exchange enhanced by charge and orbital order in $La_{0.875}Sr_{0.125}MnO_3$ [62]) and (iii) superexchange FM in compounds without Mn^{4+} ions, for instance in $La_{0.85}Pb_{0.15}Mn_{0.85}Ti_{0.15}O_3$ [63].

3.1.2. Low temperature behaviour. At low temperatures $T \ll T_C$, spontaneous magnetization of the high-T_C manganites $La_{0.7}Sr_{0.3}MnO_3$ and $La_{0.7}Pb_{0.3}MnO_3$ follows the Bloch law $M = M_0(1 - BT^{3/2})$ for ferromagnetic spin-wave excitations fairly well. Spin stiffness constants are $D = 150$ meV Å^2 [64] and 133 meV Å^2 [65], respectively.

Figure 5 gives a typical example of magnetization loops measured along the different crystallographic directions in an epitaxial (quasi-single crystalline) film. For ferromagnetic single crystals, the spin-only magnetization of 4 μ_B (3 μ_B) expected for free Mn^{3+} (Mn^{4+}) ions agrees fairly well with experimental observations of saturated magnetization, indicating the quenching of orbital moments. Coercive fields

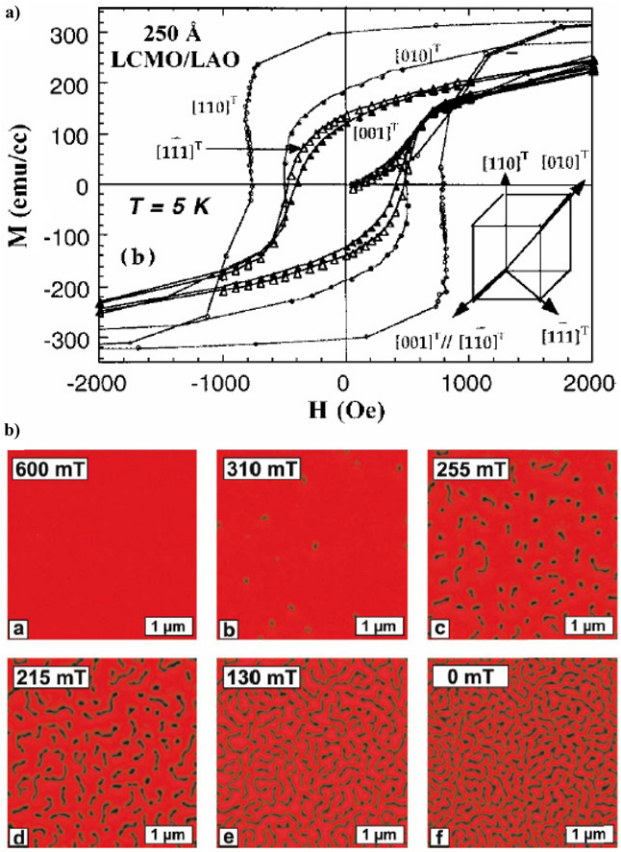

Figure 5. (*a*) Magnetization loops at 5 K of a $La_{0.8}Ca_{0.2}MnO_3/LaAlO_3(001)$ film measured along the four crystallographic directions indicated at the pseudocubic unit cell. The easy direction ($[110]^T$) is oriented perpendicularly to the film plane as a consequence of compressive strain from the substrate. (Adapted with permission from [182], ©1999 AIP.) (*b*) Evolution of domain structures in a $La_{0.7}Sr_{0.3}MnO_3/LaAlO_3(001)$ film recorded along the decreasing branch of the major hysteresis loop by magnetic force microscopy. (Reprinted with permission from [66], ©2004 APS.)

of a few millitesla are commonly found in crystals and less strained films; the rather low value is related to the low magnetocrystalline anisotropy of manganites. For the same reason, thin films tend to show dominating stress-induced anisotropy (5.3) including a possible change in the easy axis direction (figure 5) [66]. The domain size and domain wall width in bulk single crystals have been investigated by magnetic force microscopy (MFM) and Kerr Microscopy (5.2).

3.2. Spin glasses and cluster glasses

3.2.1. Fundamentals. Spin glasses (SGs) have been described and analysed in detail by Mydosh [67]. Classical examples are CuMn and AuFe. A SG is microscopically characterized by the presence of (i) sufficiently strong, competing magnetic interactions and (ii) randomness. When a SG is cooled down, a process called 'collective freezing' of magnetic moments at a magnetic glass temperature T_g is observed. Magnetic interactions are stronger than thermal activation below T_g, thus magnetic moments are immobile. The ground state is an arrangement of magnetic moments without a long range order which, however, may have a net (spontaneous) magnetization. Near and below T_g, SGs show a very slow response to changes of an external magnetic field. This is related to the observed strong irreversibility of magnetization measured, e.g. after field cooling (FC) or zero field cooling (ZFC) of a sample.

Magnetic clusters are found when a ferromagnet is dispersed in small droplets within a non-magnetic matrix (e.g. in Co–SiO_2 granular films). Similarly, several magnetic moments might be ferromagnetically coupled in a cluster surrounded by a magnetic environment with weaker or AFM interactions. A single ferromagnetic cluster of sufficient size has an intra-cluster T_C, below which it may be described as one magnetic 'super' moment (*superparamagnetic cluster*). The ground state of such a cluster system might be governed by *superparamagnetic blocking*: the cluster magnetization freezes at a blocking temperature T_B where thermal activation becomes insufficient for rotation against magnetocrystalline and shape anisotropy of the cluster. Above T_B, cluster magnetizations rotate freely as in a paramagnet; therefore, this state is called superparamagnetic. For a system of many clusters, the zero field ground state has no net magnetization since individual magnetizations of clusters cancel. The alternative case is the *cluster glass*: clusters may freeze in a spin glass-like state when magnetic interactions between clusters are strong enough.

3.2.2. Origin of disorder in manganites. There is no doped manganite without disorder, as long as two or more different ions reside on the La lattice site at random. For instance, La^{3+} and Ca^{2+} in $La_{0.7}Ca_{0.3}MnO_3$ have different ionic radii and charges. The disorder induced by radius variation on the La site has been quantified by the variance $\sigma^2 = \langle r_A^2\rangle - \langle r_A\rangle^2$. Most La site disorder is found in half-doped Ba manganites such as $Eu_{0.5}Ba_{0.5}MnO_3$ and $Gd_{0.5}Ba_{0.5}MnO_3$ since Ba^{2+} is much larger than the rare earths [68]. For some Ba half-doped manganites, ordering at the La site has been achieved [69]. Another way to introduce disorder is the partial substitution of Mn by other TMs (see below). This allows one to introduce random local magnetic coupling. Note that apart from the doping level and average ionic radius on the La (and on the Mn) site, disorder represents a third fundamental parameter governing the magnetic and the electric phase diagrams [68, 69].

3.2.3. Substitutions in the Mn sublattice. Numerous experimental studies of substitutions in the Mn sublattice are known [70–75]; some substituted TM ions are Zn^{2+}, Al^{3+}, In^{3+}, Ga^{3+}, Ti^{4+}, Ge^{4+}, Ta^{5+}, W^{6+} (non-magnetic) and Fe^{3+}, Ru^{n+} ($n = 3$, 4 or 5) and Mo^{6+} (magnetic). There is benefit from these studies for thin film multilayer structures also, as interdiffusion might produce such substituted phases at interfaces.

Microscopic consequences of other TM at Mn sites are rather multiple. This makes it commonly difficult to attribute changes of magnetic properties to a certain mechanism. (i) Deviation of ionic charge of TM and (average) Mn: this effect cannot be avoided for an intermediate Mn valence (in doped manganites). Consequently, the *number of charge carriers* changes with TM substitution. (ii) Difference of ionic radii of TM and average Mn ion: the *average ionic radius* at the Mn lattice site will change due to both, the

deviating TM ionic radius and the shifted Mn charge state upon substitution (since Mn^{4+} is smaller than Mn^{3+}). An increasing ionic radius at the Mn lattice site enhances the present distortions, since the tolerance factor is smaller than $t = 1$ for most manganites. (iii) Some TM ions *participate in magnetic superexchange* which might be ferro- or AFM. For TM = Ru, even the participation in double exchange interaction was proposed [72]). Other TMs are non-magnetic and dilute the magnetic lattice. (iv) A mechanism has been suggested concerning the effect of a deviating *local electrostatic potential*. Charge carriers are attracted or repelled by TM ions and, thereby, an increased tendency for localization arises [73]. (v) Disorder at the Mn site (variation of ionic size). (vi) Local suppression of the JT effect since most substituted TM ions are non-JT ions.

Here, some general features of magnetic behaviour for the Mn site substituted ferromagnetic manganites are summarized, restricted to the case where the unsubstituted compound is near the optimum doping level. If this is not fulfilled, an enhancement of T_C or even a modification of an insulating antiferromagnet to a ferromagnetic metal by Mn site substitution is possible, provided the charge carrier density is shifted appropriately. In most studies of such ferromagnetic $(R, A)(Mn,TM)O_3$, T_C decreases with an increasing degree of substitution. The metal–insulator transition temperature T_{MI} drops with a rate similar to T_C for low-level substitutions but disappears at a certain level y_1 ($y_1 < 0.2$ for most TM ions). For $y > y_1$, a ferromagnetic insulating state appears. At a certain higher degree of substitution $y_2 > y_1$, the collinear ferromagnetic order is lost in the ground state (visible by a lack of magnetic saturation). For compounds with $y \geqslant y_2$, spin-canted and clustered magnetic structures have been discussed [74, 75]. Typically, these compounds show slow dynamics of magnetization, history dependence and other features of spin- or cluster glasses.

3.2.4. Experiments on SG like manganites. In a standard experiment, the sample is zero-field-cooled ($H = 0$) to $T_0 < T_g$ and the magnetization is measured during warming up in a constant moderate magnetic field (*ZFC run*). In a second run, the cooling is done in the magnetic field (*FC run*). A pronounced splitting of both curves appears near the glass (or superparamagnetic blocking) temperature where thermal movement of magnetic moments 'freezes out'. Larger measuring fields reduce the splitting.

A slow dynamics of spins is observed in the *time-dependent magnetization* (M) after an applied magnetic field has been changed. For instance, the decay of remanent ($H = 0$) magnetization after field cooling a sample to a temperature $T < T_g$ can be recorded. Another experiment starts with ZFC of the sample to $T < T_g$ where it is kept for a waiting time t_W before the time dependence of M in the moderate magnetic field is recorded. This experiment allows one to detect the *ageing* of the sample: interactions between the frozen magnetic moments at $H = 0$ will slowly change the magnetic state. Ageing experiments help in distinguishing between superparamagnets (no ageing) from glassy samples. Sometimes, logarithmic relaxation typical for a very broad distribution of individual relaxation times is observed. Other types of SG relaxation are power-law-like, exponential or stretched exponential, depending on the distribution of energy barriers in the system.

At about the glass temperature T_g, a sharp cusp-like peak appears in the linear *AC susceptibility* χ, which is reduced and shifted to a higher temperature with increasing frequency [67]. Historically, the sharp anomaly observed at T_g in canonical SGs triggered the idea of a distinct phase transition at T_g (still under discussion). For further analysis, the imaginary part of the susceptibility, χ'', and the non-linear contribution χ_3 are studied [67, 75, 76].

The *heat capacity* of SGs has an approximately linear magnetic contribution $C_{mag}(T) = \beta T^n$ with $n \sim 1$ below T_g and a maximum of C_{mag} just above T_g [67].

Neutron diffraction is applied to search for a long-range magnetic order. However, due to the resolution limit, the absence of the long-range order is difficult to prove. Spin-polarized neutrons in a neutron depolarization experiment can detect magnetic clusters or domains (100 nm–50 μm) possessing a net magnetization with a high sensitivity [74]. Smaller clusters can be investigated by small angle neutron scattering (SANS) [77].

3.3. Rare earth magnetism

Most rare earth elements on the La site of manganites have a magnetic moment and their own magnetic ordering phenomena, typically below 50 K. For the heavy rare earth elements Ho–Lu, $RMnO_3$ has a non-perovskite hexagonal lattice structure [78]. (Most of the hexagonal phases are *ferroelectric*.) In perovskite phases, R–Mn magnetic coupling (being stronger than R–R coupling) might be AFM and/or cause spin reorientation transitions since a reduced or even a negative value of M is found at a low temperature in particular for R = Nd [65, 79, 80]. Some neutron diffraction studies of magnetic structures have been done, particularly for R = Nd [80–83]. The rare earth may induce strong magnetic anisotropy as for the case of $PrMnO_3$ [84]. A Schottky anomaly arises in the heat capacity of $RMnO_3$ from the exchange or crystal-field splitting of R energy levels [65, 84–86].

4. Electric transport: intrinsic properties

4.1. CMR: experimental features

In section 4, the typical resistive behaviour of FM single crystals is addressed. It is restricted to *metallic* manganites in the sense of $d\rho/dT > 0$, with resistivity ρ and temperature T. Epitaxial films on single-crystalline substrates show similar transport properties such as single crystals, possibly altered by strain and the influence of finite thickness (see 5.3). No details of field- or light-induced metallic conduction in CO phases are included.

The characteristic transport behaviour is illustrated by the temperature dependence $\rho(T, H_0)$ at $H_0 = 0$ and 5 T of a $La_{0.7}Ca_{0.3}MnO_3$ sample (figure 6). At low temperatures, the resistance follows an expression $\rho = \rho_0 + \rho_1 T^\alpha$ with α = 2–2.5. The temperature-dependent term has been attributed to the electron–electron scattering or first-order electron–magnon scattering (for both, $\alpha = 2$), while in a real half-metal only the second order electron–magnon processes are allowed ($\alpha = 4.5$) [18]. The residual resistivity ρ_0

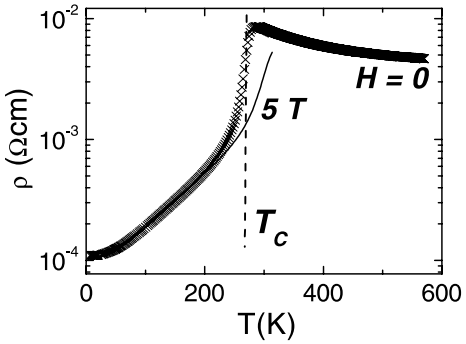

Figure 6. Resistivity in dependence on temperature of a ferromagnetic $La_{0.7}Ca_{0.3}MnO_3$/$LaAlO_3$(001) epitaxial film, measured in a magnetic field $\mu_0 H = 0$ and 5 T. T_C indicates the ferromagnetic Curie temperature. Large magnetoresistance is observed in the vicinity of T_C associated with a metal-insulator transition.

is large if compared with elemental metals, with minimum values of about $\rho_0 = 40\,\mu\Omega\,\mathrm{cm}$ (for $La_{0.7}Sr_{0.3}MnO_3$), and several orders of magnitude higher values for some FM manganites. This mainly reflects the low mobility of charge carriers, since their density is not much smaller than in elemental metals. Low-temperature *MR* vanishes for high-quality crystals with a collinear ferromagnetic structure, since thermal spin fluctuations are negligible.

Near T_C, ρ strongly increases and shows a peak at a metal–insulator transition temperature $T_{MI} \sim T_C$. In the paramagnetic state, charge transport is thermally activated (apart from a few large-band-width Sr manganites which are paramagnetic metals). In other words, the ferromagnetic order changes the character of the electron transport from activated to metal-like. In a temperature range around T_C, ρ drops considerably upon application of a magnetic field of few tesla (figure 6). This large negative MR effect has been called 'CMR' in analogy to GMR; it is larger than GMR but also needs much larger fields. Why does such sensitivity of resistance to magnetic fields (being moderate in comparison to the thermal energy kT) appear in manganites? This might be the central question of manganite physics.

Above T_C, the observed activated behaviour is consistent with small adiabatic polaron hopping $\rho(T) = AT\exp(E_{hop}/kT)$ [87] in epitaxial films of $La_{0.7}Ca_{0.3}MnO_3$ (figure 6) [88] and in some high-quality crystals. In other samples (some single crystals and polycrystals), Mott variable range hopping (VRH) $\rho(T) = A\exp[(E/kT)^{1/4}]$ has been observed [20, 89]. Even simple thermal activation $\rho(T) = A\exp(E/kT)$ gives a correct description for some samples in a certain range $T > T_C$.

An early, simple CMR model (see 4.2) gives an analytical expression for $R(H)$: a magnetization-dependent energy barrier is assumed for activated transport [20, 89, 90]. This leads to well-defined relations between R and M, such as $R \propto -M$ (or $R \propto \exp(-M)$) in the FM state and $R \propto -M^2$ (or $R \propto \exp(-M^2)$) in the PM state which have indeed been observed occasionally [91, 92]. Furthermore, $M(H,T)$ has been successfully approximated by a Brillouin function according to mean field theory for some cases, leading to an expression for $R(H)$ [90]. The agreement between the data and Wagner's model is found to be reasonable in the PM regime and in a certain temperature range below T_C [90, 93]. Deviations are most pronounced close to T_C and for lowest temperatures where the transport is no longer well described by the thermally activated hopping.

4.2. CMR: models

More detailed information is found in the reviews [18, 21, 30, 94]. Here, the essential mechanisms are outlined in a phenomenological way.

4.2.1. Ferromagnetic double exchange. Obviously, FM double exchange interaction provides a strong correlation between magnetic order and electron transport. This is reflected in the expression for the (semiclassical) electron transfer probability between two Mn ions $t = t_0\cos(\Theta/2)$, with the angle Θ between the Mn magnetic moments [24]. Experimentally, this correlation is visible in the interrelation between R and M (figure 7). Early models assume hopping of electrons between FM regions (single Mn ions or ferromagnetic clusters of Mn ions) with a magnetic energy barrier proportional to $(1 - \boldsymbol{M}_1 \cdot \boldsymbol{M}_2)$, with the normalized magnetizations $\boldsymbol{M}_1$, $\boldsymbol{M}_2$ at the start and end points of the hopping process [89, 90]. Indeed, these hopping models (VRH, small or large polaron hopping, simple activation) have obtained quite reasonable agreement with the data of temperature dependence $R(T)$ and field dependence $R(H)$ of resistance of several manganites (see 4.1).

Double exchange has been agreed as being crucial for CMR but insufficient to explain the phenomenon. Several theoretical approaches based on double exchange models reproduce neither the appearance of a metal–insulator transition nor the size of CMR, in particular for the low-T_C compounds where CMR is really huge. For details on some calculations, see [21, 30]. The large-band-width manganites such as $La_{1-x}Sr_xMnO_3$ ($x \sim 0.25$–0.4) seem to be closest to pure double exchange systems.

4.2.2. JT polarons. The polaron-like transport behaviour of $\rho(T)$ observed for $T > T_C$ (e.g. [87, 88]) indicates that polarons are the predominant high-temperature type of charge carriers in manganites. While earlier work proposed *magnetic* polarons, i.e. a magnetic polarization of Mn spins surrounding a moving electron [35], elastic lattice polarons originating from the strong JT effect of Mn^{3+} ions were recognized as an essential mechanism later [27, 87]. For localized e_g electrons, the JT distortions of oxygen octahedra around $Mn^{3+}$are static and typically collective (orbital order). These distortions become dynamic when e_g electrons move. Then, charge carriers might be trapped by the local lattice distortion that they produce, forming localized lattice polarons. Millis included the JT electron–phonon coupling and double exchange in a mean-field calculation and obtained M–I transitions and CMR in qualitative agreement with experiments [27, 95–97]. The importance of electron–phonon coupling for manganite physics is generally accepted now.

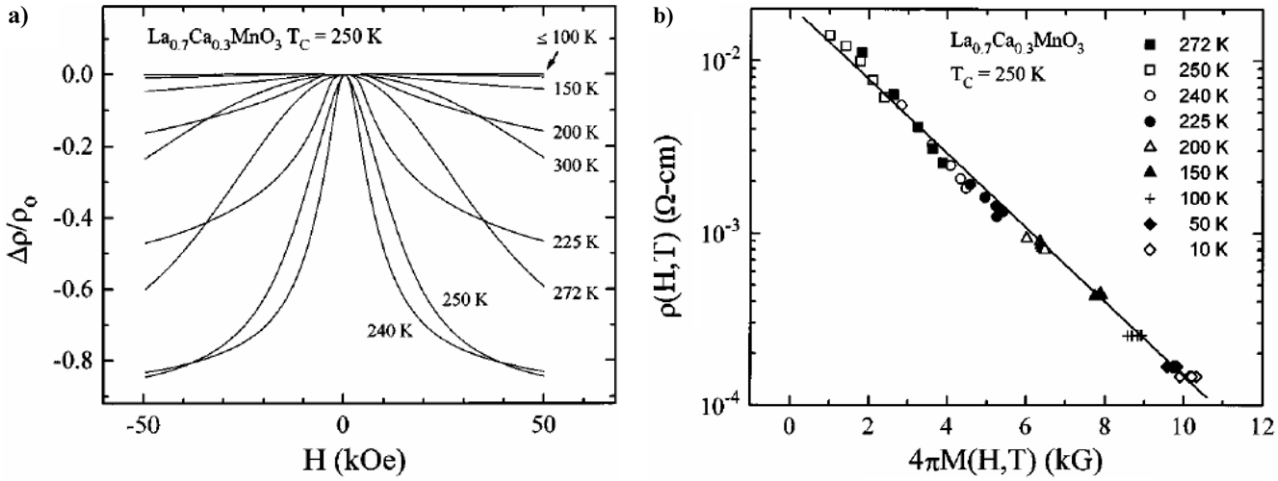

Figure 7. (*a*) Magnetoresistance $\Delta\rho = \rho(H) - \rho_0$ versus magnetic field of a $La_{0.7}Ca_{0.3}MnO_3$ epitaxial film at constant temperatures above and below the ferromagnetic Curie temperature T_C. (*b*) The resistivity scales logarithmically with the magnetization of the film for all recorded temperatures, giving the evidence of a strong correlation between resistance and magnetic order. (Adapted with permission from [92], ©1995 AIP.)

4.2.3. Percolation in a phase-separated state. Several experiments (see 2.6) have revealed another striking property of some manganites: the coexistence of nanoscale regions representing different phases (with extensions varying from 1 to more than 1000 nm, depending on the composition). This includes the coexistence of metallic and insulating regions or regions of very different electric conductivity. Thus, the idea of a percolation mechanism of CMR arose. Individual sample regions would change from a metal to an insulator state depending on external parameters such as T and H, showing a broad distribution of T_{MI} in phase-separated samples. (Further parameters such as x-ray or light irradiation, large current or strong electric field can also induce insulator-to-metal transitions (2.6) and, thus, alter the phase distribution in a PS state.) Extended numerical studies by Dagotto and coworkers [21,98] on simulated random resistor networks found M–I transitions having a strong resemblance to the experimental results. An earlier mixed-phase approach was suggested by Salamon *et al* [94] who have adjusted the temperature-dependent volume fractions of a metallic phase and a polaronic insulator phase to consistently describe resistance and thermopower measurements. While for certain compounds, e.g. $Pr_{0.7}Ca_{0.3}MnO_3$ and some other Pr manganites, the presence of phase separation and its dominating role for CMR is rather generally accepted, many open questions remain. For instance, how general is the percolation mechanism of CMR, and are there manganites showing CMR without phase separation? What parameters govern the length scale of phase separation—might this be a disorder parameter? Is there any way to give analytical expressions for the field dependence of CMR?

4.2.4. Critical fluctuations. Murakami and Nagaosa suggested that (one type of) CMR might originate from enhanced fluctuations near a multicritical point [99]. Strong fluctuations may result in an unusually strong sensitivity of properties to a magnetic field. The schematic phase diagram reproduced in figure 8 reveals a multicritical point for $R_{0.5}Ba_{0.5}MnO_3$ where the CO state obtained for smaller R ions changes the ferromagnetic metallic (FM–M) state for larger R ions. (The R ionic radius tunes the electronic band width, see 2.6.) Near this multicritical point, a very large CMR has been measured [100]. Similar multicritical points are present in other classes of manganites where CO and FM–M phases exist. Note that the continuous (second order) phase transition at T_C becomes first order near the multicritical point. As pointed out in 3.1, there are low-T_C manganites with large CMR but continuous phase transition, which seem to be different, indicating that disorder might be an essential parameter. For $R_{0.5}Ba_{0.5}MnO_3$ compounds it is possible to 'switch' the amount of disorder by ordering R and Ba ions on the La site into a layered superstructure [69]. Hence, ordered and disordered versions of the phase diagram (figure 8) have been established. The disordered FM compounds have a lower T_C. Note that the charge order is completely replaced by a SG state for the disordered compounds. Again, a multicritical point appears between SG and FM, and it is again associated with the large CMR. However, phase separation might be absent for the disordered compounds down to a length scale of 2 nm as found for $Eu_{0.5}Ba_{0.5}MnO_3$ [100]. Note further that by increasing the disorder one can turn (i) a first order PM–FM transition into a second order and (ii) a CO manganite into a ferromagnetic, according to a phase diagram as that shown in figure 8.

5. Thin films: preparation and properties

Thin films below 1 μm thickness are essential for applications in microelectronic devices where lateral structuring, e.g. by lithography is employed to produce nanometre-size functional elements. On the other hand, thin films are also important for fundamental research: they allow us to study the effects of finite thickness, biaxial strain, interface electronic structure and proximity effects, just to mention some issues. Since thin film growth is far from equilibrium conditions, new phases can be obtained. Epitaxial films may have very high

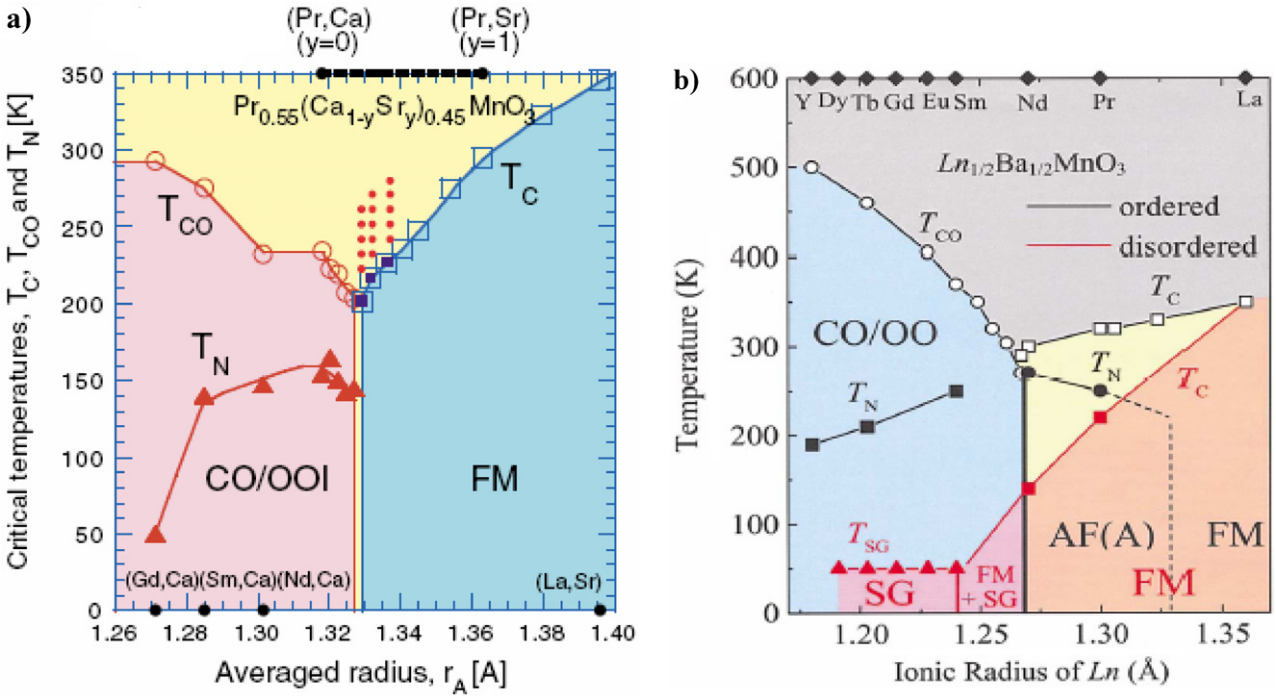

Figure 8. Magnetic phase diagrams as a function of the averaged ionic radius on lattice A site of single-crystalline (*a*) $Pr_{0.55}(Ca,Sr)_{0.45}MnO_3$ and (*b*) $Ln_{1/2}Ba_{1/2}MnO_3$ with Ln = La–Dy and Y. The half-doped Ba manganites were prepared with ordered or disordered Ln/Ba sublattice. Multicritical points exist between CO/OO and FM phases and between FM and SG phases. The magnetoresistance of FM phases is particularly large near the multicritical points. Abbreviations are FM—ferromagnetic metal, CO/OO—charge and orbital ordered, I—insulator, SG—spin glass, T_C—ferromagnetic Curie temprature, T_N—Néel temperature, T_{CO}—charge ordering temperature and T_{SG}—glass temperature. (Reprinted with permission from [69] (left panel) and [99] (right panel), ©2003 APS.)

crystalline quality, comparable to single crystals. For reviews on manganite thin films, see [101–103].

5.1. Preparation and lattice structure of films and multilayers

5.1.1. Preparation. Epitaxial oxide films have been prepared since about mid-1980s when sputter techniques and laser deposition, e.g. for cuprate superconductors, were developed [104, 105]. First results on manganite films have been published by Chahara [106], von Helmolt [7] and Jin *et al* [107]. Early work was done employing ion beam sputtering or pulsed laser deposition (PLD) from a ceramic target of nominal composition. Typical deposition conditions include substrate temperatures between 580 and 900 °C, oxygen background pressure of up to 0.1–0.5 mbar (or less for methods related to molecular beam epitaxy (MBE)) and growth rates down to 0.1 Å s^{-1}. Meanwhile, a variety of preparation methods have been used: magnetron or ion beam sputtering [106, 108, 109], PLD [7, 110–112], Laser-MBE [113–115], MOCVD [116], sol–gel methods [117] and metal-organic aerosol deposition [118].

Epitaxial growth has been proved possible on oxide single-crystal substrates of MgO(100), $SrTiO_3$, $LaAlO_3$, $NdGaO_3$, YSZ(100) (Y-stabilized ZrO_2) [119], $(LaAlO_3)_{0.3}(Sr_2AlTaO_6)_{0.7}$ (LSAT) [120] and PMN-PT(001) $(PbMg_{1/3}Nb_{2/3}O_3$–$PbTiO_3)$ [121]. Table 1 lists the composition and lattice parameters of the substrates. Epitaxy on Si is more complicated but has been achieved by several groups using buffer layers (e.g. [122, 123]). Direct Si/$SrTiO_3$ epitaxy was demonstrated by McKee *et al* [124] as a promising step towards introduction of perovskite oxides to silicon technology (as dielectrics with high dielectric constant), even though rather high phase formation temperatures of oxides may pose another problem.

Table 1. Typical materials of monocrystalline substrates employed for epitaxial growth of manganite films, pseudocubic lattice parameter and electric classification. For an example of thin film growth on PMN–PT see [121].

Composition	Lattice parameter (Å)	Properties
$LaAlO_3$	3.79	dielectric
$0.3LaAlO_3$–$0.7Sr_2AlTaO_6$ (LSAT)	3.87	dielectric
$SrTiO_3$	3.905	dielectric
Y : ZrO_2 (YSZ)	4.18	dielectric
MgO	4.20	dielectric
$NdGaO_3$	3.863	dielectric, magnetic
Nb : $SrTiO_3$	∼3.91	conducting
$0.72Pb(Mg_{1/3}Nb_{2/3})O_3$–$0.28PbTiO_3$ (PMN-PT)	∼4.02	ferroelectric, piezoelectric

Monitoring film growth as usual, e.g. by *in situ* RHEED, is complicated for a high oxygen pressure of the order of 10^{-1} mbar. Therefore, films may be deposited under lower pressure (as done for Laser-MBE). Alternatively, a high-pressure RHEED facility developed by Rijnders *et al* [125, 126] allows one to monitor the layer-by-layer growth of oxide films. This technique gave important information

on growth mechanisms like surface diffusion times of ions impinging on the substrate, and led to proposals of improved deposition timing (choice of frequency, waiting times) for high crystalline quality (*interval deposition* method [127]).

As-grown films may be oxygen-deficient: typically, reduced values of T_C and T_{MI} were found in early work. Soon it was realized that post-growth annealing of films in oxygen or air may increase transition temperatures and reduce the resistance of grown films (sometimes by a factor 10–100). However, annealing may have several effects: while an oxygen deficiency is compensated (or over-compensated, introducing metal vacancies to the lattice), recrystallization and stress-relaxing defect formation may occur depending on the annealing temperature. Thus, strain release is another common result of thermal annealing, with strong influence on magnetic properties of films (section 5.3). Oxygen diffusion is known to be relatively easy in oxide perovskites, including cuprate superconductors. Vacuum annealing at a temperature of 400 to 500 °C can be used to remove oxygen and study properties resulting from O deficiency (essentially described by the change in the Mn oxidation state) [128]. Reoxygenation occured even below 100 °C.

Most deposition methods are capable of *in situ* multicomponent growth using several targets. Perovskite-like oxides with a pseudocubic lattice constant of about 3.7–4.0 Å, including those oxides used as substrates, may be grown in heteroepitaxial multilayers if no chemical incompatibility is present. Thus, tunnel trilayers of conducting manganites and insulating $SrTiO_3$ have been prepared [15, 129, 130] (section 6.2). Periodic alternating multilayers of two components have been grown by several groups. If epitaxial, they form crystallographic superlattices (figure 9). Examples are $[La_{0.7}Sr_{0.3}MnO_3/SrTiO_3]_n$ [131], $[La_{0.6}Sr_{0.4}MnO_3/La_{0.6}Sr_{0.4}FeO_3]_n$ [110], $[LaMnO_3/SrMnO_3]_n$ [132], $La_{0.7}Ca_{0.3}MnO_3/Al_2O_3$ (non-epitaxial) [133], $SrO/(La,Sr)MnO_3$ (artificial construction of the Ruddlesden-Popper phase $(La,Sr)Mn_2O_7$) [113], $[PrMnO_3/SrMnO_3]$ [115] and $[LaSrMnO_3/YBa_2Cu_3O_7]$. Further oxides in multilayers with manganites include $SrRuO_3$, $CaTiO_3$ (the perovskite), ferroelectrics $(Ba,Sr)TiO_3$ and $Pb(Zr,Ti)O_3$ (section 7), and some cuprate superconductors. Furthermore, epitaxy with Pt metals seems possible since it has been achieved on $SrTiO_3(001)$ [134].

Fabrication of small lateral structures is reviewed by Haghiri–Gosnet [101]. A comfortable technique for larger structures (200 μm) is based on shadow masks used during deposition [133, 135, 136]. Photolithography combined with chemical etching or ion milling can define structures down to about 1 μm width. Electron beam lithography [101] and focused ion beam (FIB) [137] were used to fabricate lateral nanostructures down to below 100 nm.

5.1.2. Lattice structure. Substrates with cubic lattice commonly induce a tetragonal distortion to an epitaxially grown film. (As an exception, for larger lattice misfit, dislocation formation at the interface may be followed by unstrained growth of the film [138].) Additionally, the film may be split into structural domains of different lattice orientation for orthorhombic or rhombohedral compounds [139]. X-ray diffraction (XRD) is the most employed technique for the investigation of crystallographic lattice structure of films. (Neutrons are rarely used since films have too low volume.) Phase purity, lattice orientation and approximate out-of-plane lattice constants of films are determined by standard XRD in Bragg–Brentano (Θ–2Θ) geometry. Shifts of the out-of-plane lattice constant with respect to the bulk value indicate the strain state of films. In-plane texture can be characterized by ϕ scans or pole figures and strain states by reciprocal space mapping. Periodic multilayers show superlattice reflections around the main peaks [131], with their intensity related to the interface roughness [140].

5.2. Microstructure, magnetic domains and other local properties

In this paragraph, some results obtained by local probes techniques on manganite films are collected, although it is far from being representative for this wide research area.

5.2.1. TEM: microstructure down to the atomic level. There are a number of investigations of local lattice structure and interface structure by TEM, e.g. [139, 141–143] (figure 9). Distortions from original bulk symmetry have been investigated for $La_{1-x}Ca_xMnO_3/SrTiO_3(100)$ [141, 143]. Up to a critical thickness, epitaxial films usually grow coherently strained. Thicker films may have a two-layer structure of a coherently strained bottom layer and a (partially) strain-relaxed, possibly defect-rich upper layer, both separated by a defect-rich zone (figure 9(*d*)) [142, 143]. For MgO(001) substrates with large lattice misfit, dislocations reside directly at the substrate-film interface [138]. In superlattices, coherent interfaces of manganites (such as $La_{0.7}Sr_{0.3}MnO_3$) with dielectric oxides (such as $SrTiO_3$) have been found, irrespective of the interface roughness. It has been proved for $La_{0.7}Sr_{0.3}MnO_3/SrTiO_3$ that very smooth interfaces (with low interdiffusion checked by electron energy loss spectroscopy (EELS) [144, 145]) can be obtained [142, 145].

5.2.2. Scanning tunnelling techniques (STM, STS, STP). STM and scanning tunnelling spectroscopy (STS) have provided some important results on the inhomogeneous distribution of metal and insulator phases (phase separation) in strained manganite films [39–41]. The local metal or insulator character is derived from current-voltage (I–V) characteristics measured at the tip position. Since the underlying process is electron tunnelling, few atomic layers at the surface are probed. Fäth *et al* [39] recorded magnetic-field-induced changes in the phase distribution. The surface topology can be imaged simultaneously with high resolution (down to atomic level) [41]. Spin-polarized STM was demonstrated by Akiyama *et al* with a PtIr tip covered by $La_{0.7}Sr_{0.3}MnO_3$ [146]. Scanning tunnelling potentiometry (STP) is employed to map the local distribution of the electric potential arising when a current/voltage is applied to the sample [147]. Steps in the local potential were detected at GB (demonstrating their high resistance) and at step edges [148].

5.2.3. Atomic force microscopy (AFM): surface topology. This technique is widely used to check the surface of films after preparation (e.g. [125, 126]). It has a lateral resolution

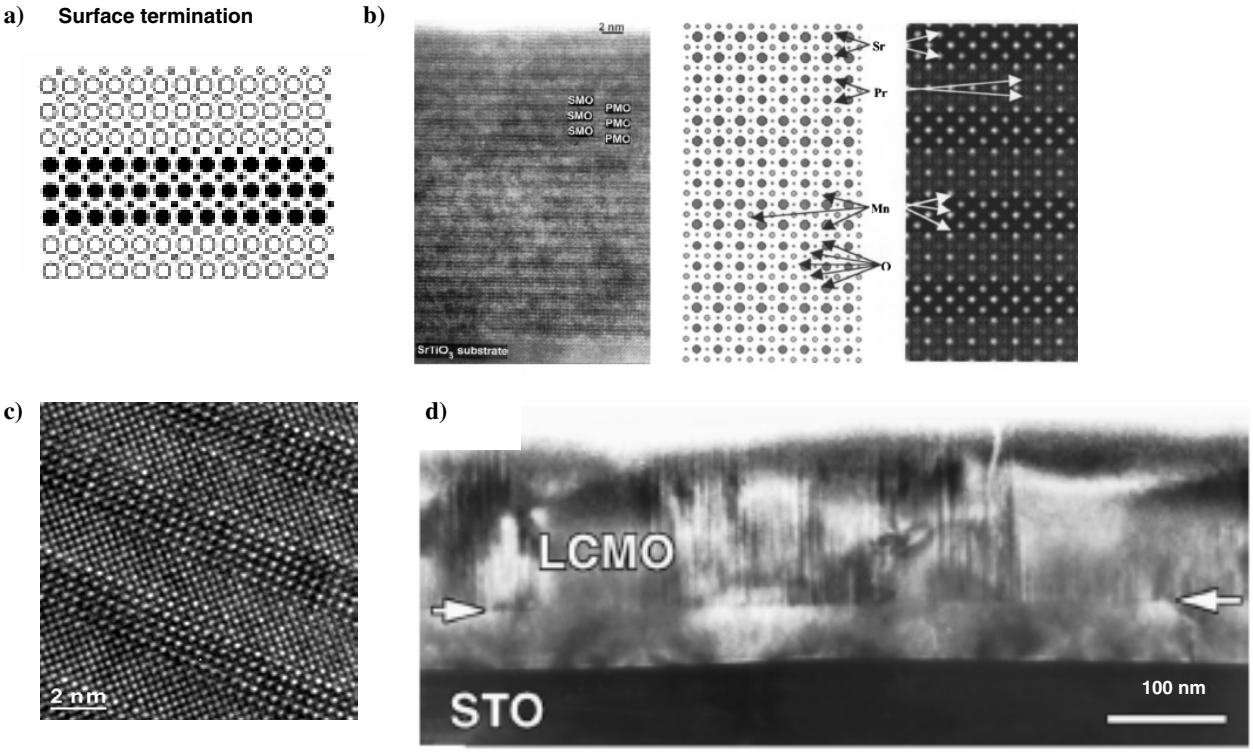

Figure 9. (*a*) Epitaxy of two perovskites $ABO_3/A'B'O_3$ can create two distinct interface types ($AB'O_3$ or $A'BO_3$) depending on the surface termination (A or B) of the lower layer. (Adapted with permission from [110], ©1999 Elsevier.) (*b*) High-resolution transmission electron microscopy (HRTEM) image of a heteroepitaxial multilayer of alternating $SrMnO_3$ and $PrMnO_3$. (Reprinted with permission from [115], ©2003 AIP.) (*c*) HRTEM of a coherent $La_{0.7}Sr_{0.3}MnO_3/SrTiO_3$ multilayer (courtesy of K Vogel and H Lichte). (*d*) Cross section of a $La_{2/3}Ca_{1/3}MnO_3/SrTiO_3(001)$ film with an internal interface separating a coherently strained lower layer from an upper layer showing columnar growth. (Reprinted with permission from [143], ©1998 APS.)

of several nanometres, well below grain sizes in films. The vertical resolution can be very good (below 1 Å), depending on tip quality and noise level. The average rms (route mean square) or peak-to-valley roughness are given to characterize a grown film. Line scans on smooth films reveal surface steps of the height of one pseudocubic unit cell, indicating one stable termination out of the two possible ones for the perovskite lattice [126].

5.2.4. MFM: magnetic domains. MFM has been applied to image magnetic domains of manganites with a resolution down to ∼30 nm [149–152]. Usually, the perpendicular component of the local magnetization is recorded. Compressively strained films of $La_{0.7}Sr_{0.3}MnO_3/LaAlO_3(100)$ show strain-induced magnetization perpendicular to the film plane, with a domain size of about 200 nm [149]. In a similar film, Schwarz *et al* [66] visualized the magnetization reversal (Barkhausen effect) of a large number of domains and studied domain nucleation behaviour. Soh *et al* [151, 152] discovered a prevailing grain boundary magnetization above the volume T_C in strained $La_{0.7}Sr_{0.3}MnO_3/SrTiO_3$ films. Pinning of domain walls at crystallographic twin boundaries has been investigated by Popov *et al* [153].

5.2.5. Magneto-optical techniques. Magneto-optical techniques applied to manganite films include Kerr microscopy and spectroscopy [154–156], sometimes using a garnet indicator film covering the sample [155, 157], magneto-optic ellipsometry [158] and second harmonic generation (SHG) [159, 160]. Pump–probe Kerr spectroscopy [161] allows one to investigate magnetic surface dynamics in the picoseconds range. Domain structure (also antiferromagnetic domains [162]) and (spin-polarized [157]) absorption/transmission spectra in dependence on incident light wavelength and polarization, temperature and applied magnetic field are major objects of investigation. Note that light can excite charge carriers in insulating manganites and create short- or long-lived local conducting states [45].

5.2.6. Photoemission spectroscopy (PES), UPS and XPS. Photoemission, such as tunnelling spectroscopy, measures surface properties with a probing depth of a few atomic monolayers. This brings about a strong influence of surface contaminations (such as carbon). Considering the high oxygen mobility in oxide perovskites, appropriate surface treatment in vacuum prior to measurements is a challenging problem. Single crystals might be cleaved. Thin films, if not prepared *in situ*, are transported to the vacuum chamber and are subject to cleaning/annealing procedures [163–165]. Several groups have reported on deviating stoichiometry of film surfaces for Sr, Ca and Pb doped $LaMnO_3$ (for instance, [164–167]), but no general trend could be confirmed yet, such as segregation

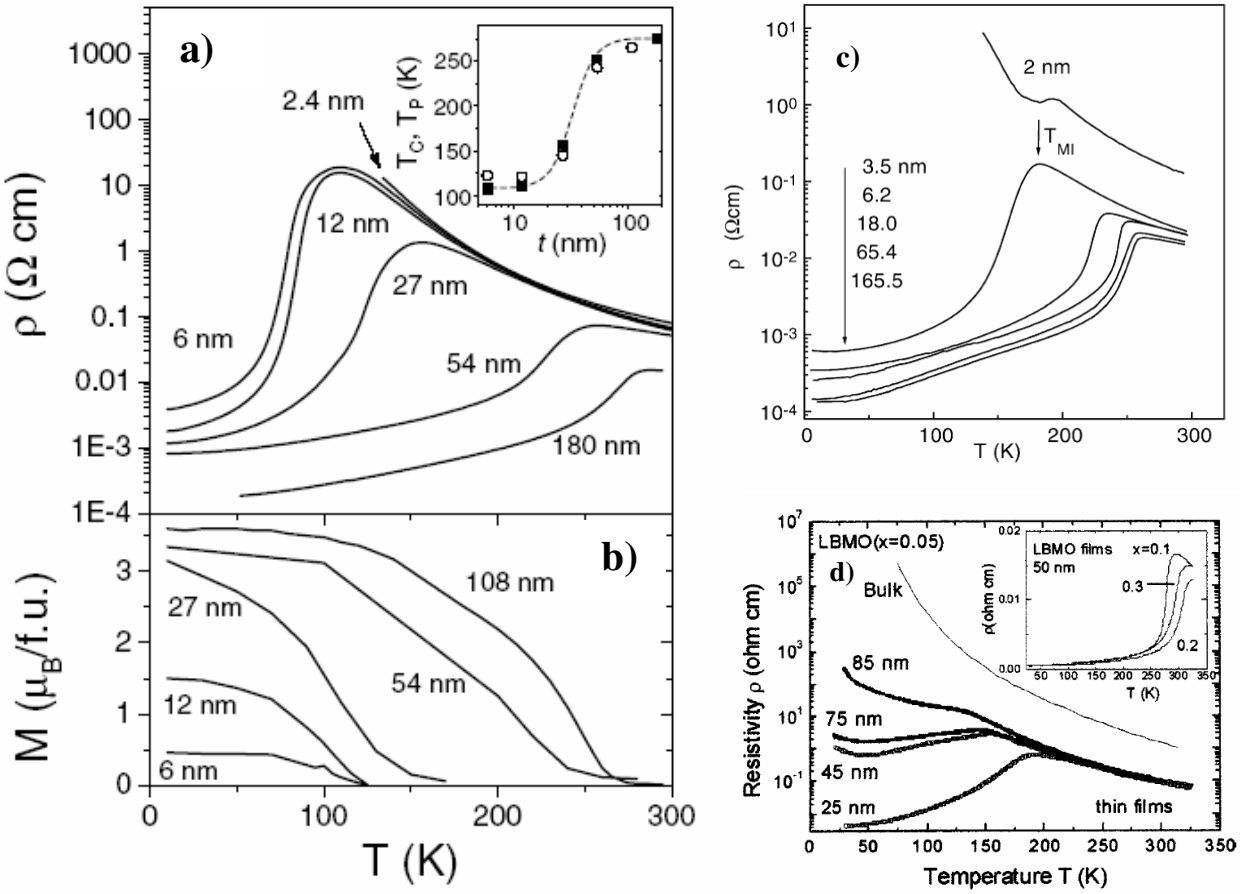

Figure 10. (*a*) Resistivity and (*b*) magnetization of epitaxial $La_{0.67}Ca_{0.33}MnO_3/SrTiO_3(001)$ films of varing thickness. Inset of (*a*): thickness dependence of the metal-insulator transition temperature (T_P) and ferromagnetic Curie temperature. (Both (*a*) and (*b*) adapted with permission from [174], ©2001 APS.) (*c*) Resistivity versus temperature of $La_{0.7}Ca_{0.3}MnO_3/NdGaO_3$ low-strain films. (Reprinted with permission from [172], ©2000 Elsevier.) (*d*) Thin $La_{0.95}Ba_{0.05}MnO_3$ films on $SrTiO_3(001)$ substrate are metals, contrary to insulating bulk behaviour. An enhancement of conduction and metal-insulator transition by tensile strain as observed in this case is exceptional for manganite films. (Adapted with permission from [177], ©2001 APS.)

of large alkali ions. Park *et al* [168, 169] observed the half-metallic character of a $La_{0.6}Sr_{0.4}MnO_4$ film surface by spin-resolved photoemission (SPES).

5.3. Magnetic and electric properties of films (effects of film thickness and strain)

Early publications on thin films of FM manganites revealed a rather wide spread of T_C and resistivity values for nominally equal samples with respect to the film–substrate combination, revealing a strong influence of the microstructure. Meanwhile, numerous studies have addressed thickness-dependent properties of films from about 2 to 200 nm (e.g. [170–174]). For film thickness $d > 150$–200 nm, films typically behave similarly to bulk material since epitaxial strain has been relaxed by defect formation in a substrate-near layer. Finite size (thickness), biaxial strain and oxygen content have been recognized as parameters governing the thickness-dependent behaviour and will be discussed in the following.

Typically, thin films show a decrease in T_C and T_{MI} with decreasing thickness [120, 131, 170–173] (figure 10). The metallic character is lost below a critical film thickness. This originally led to the proposal of a 'dead layer' characterized by low magnetic order and low electric conductivity at the surfaces of a manganite film [173]. However, all three above mentioned parameters might influence the properties of such ultrathin (<10 nm) films.

The effect of *finite thickness* has been addressed for some series of low-strain films [120, 175]. Low strain has been achieved by low lattice mismatch of film and substrate, for instance in $La_{0.7}Ca_{0.3}MnO_3/NdGaO_3$ [172], $La_{0.7}Ba_{0.3}MnO_3/SrTiO_3$ or $La_{0.7}Sr_{0.3}MnO_3/LSAT$ (table 1). Another way to obtain low-strain films is annealing of as-grown films at temperatures of 900–1000 °C [176]. For such film series of low-strain films, T_C was found to follow a typical scaling law, $1 - T_C/T_{C\infty} = (N_0/N)^{\lambda}$, with $T_{C\infty}$ as the value obtained in the large thickness limit, N the number of unit cell layers, N_0 the layer number for $T_C = 0$ and λ the critical exponent [120, 175]. N_0 is rather low, usually <4. Low-strain films of a thickness of 10 unit cells ($d = 4$ nm) of $La_{0.7}A_{0.3}MnO_3$ (A = Sr, Ca) are still metallic conductors. Hence, the vanishing metal character and suppressed T_C for even lower film thickness is probably rather a natural effect

of finite thickness than a consequence of pronounced intrinsic dead layers at manganite surfaces.

In certain cases of film–substrate combinations, either (i) a much stronger reduction in T_C with decreasing thickness [171, 174] or (ii) an unusual increase in T_C with reduced thickness [177] has been found. Here, *biaxial strain* of films epitaxially grown on mismatching substrates substantially alters the film properties. Millis *et al* [178] pointed out a strong intrinsic sensitivity of manganites towards biaxial lattice distortion. The strain dependence of T_C can be described for the cubic lattice with respect to bulk compression $\varepsilon_b = -1/3(\varepsilon_x+\varepsilon_y+\varepsilon_z)$ and biaxial distortion $\varepsilon_{JT}^2 = 1/4(\varepsilon_x+\varepsilon_y)^2 + 1/16\,(2\varepsilon_z-\varepsilon_x-\varepsilon_y)^2$ of the film as [178]

$$T_C(\varepsilon_b, \varepsilon_{JT}) = T_C(0,0)(1+\alpha\varepsilon_b-\Delta\varepsilon_{JT}^2) \qquad (\alpha, \Delta > 0). \quad (2)$$

ε_x, ε_y and ε_z denote the relative length changes in x, y and z direction of the film, with z perpendicular to the film plane. α denotes the derivative of T_C with respect to volume compression. For the cubic lattice, there is no linear term in ε_{JT}. 2Δ is the second derivative of T_C with respect of biaxial distortion. Equation (2) implies that biaxial distortion (ε_{JT}) always reduces ferromagnetic order, while elastic reaction of the film perpendicular to the strained film plane decides about the induced volume change, ε_b. Enhancement of T_C in a strained film is possible for dominating volume compression, as in the case of compressively strained $La_{0.9}Sr_{0.1}MnO_3/SrTiO_3(001)$ [179]. Almost all experiments on films under tensile strain show a pronounced reduction in T_C [101], of an order of 10% for 1% in-plane strain. An exception is $La_{1-x}Ba_xMnO_3$ ($x = 0.05$–0.2) on $SrTiO_3(001)$ where 20 nm thick films show a larger T_C than the bulk material [177]. Pure elastic reaction under tensile strain could not produce the bulk compression needed to explain this behaviour. The tensile strain was proposed to modify the e_g orbital occupation, favouring in-plane x^2–y^2 orbitals [177]. Similarly, Klein *et al* [180] proposed strain-induced orbital ordering in $La_{0.67}Ca_{0.33}MnO_3/SrTiO_3(001)$ under tensile strain.

Magnetic anisotropy of FM manganite films is altered considerably by stress-induced anisotropy [181–184]. Strong compression in the film plane turns the magnetic easy axis perpendicular to the film plane. Typically, magnetostriction is positive.

The thickness-dependent phase separation in ultrathin $La_{0.7}Ca_{0.3}MnO_3$ films has been investigated by Rauer *et al* [185] using spectroscopic ellipsometry. Gradual appearance of metallic phase (detected by optical charge carrier response) with decreasing temperature, even for a 2 nm thick film, was detected. Bibes *et al* [174] analysed the relative concentration of Mn ions involved in electron transport by NMR in $La_{0.67}Ca_{0.33}MnO_3/SrTiO_3$ films and, similarly, found evidence of a metal phase in globally insulating ultrathin films.

6. Extrinsic electric transport: spin-polarized tunnelling

After intrinsic electric transport of FMM manganites (observed in single crystals and epitaxial films) has been discussed in section 4, the first part of section 6 is concerned with electric transport in polycrystalline samples. Grain boundaries (GB) dominate the low-temperature resistance of polycrystalline FM–M manganites. The second part addresses electron tunnelling in epitaxial trilayer structures.

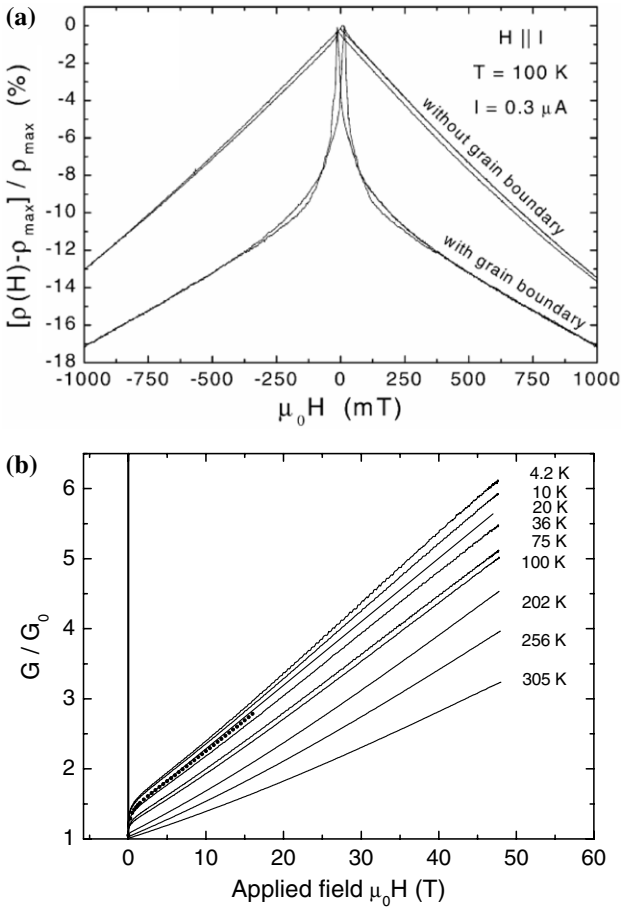

Figure 11. (*a*) Low-field magnetoresistance of $La_{2/3}Ca_{1/3}MnO_3$ with and without grain boundaries, showing the characteristic steep resistance drop in low magnetic fields from spin-dependent transport between grains. (Reprinted with permission from [192], ©2000 Elsevier.) (*b*) High-field conductance normalized to the value obtained in zero field measured on a polycrystalline non-textured $La_{0.7}Sr_{0.3}MnO_3$/YSZ(001) film. Note the nearly linear magnetoconductance at low temperatures. (Courtesy of N Kozlova.)

6.1. Grain boundaries

GB are the origin of additional resistance in polycrystalline manganites: magnetic disorder at GBs is associated with high resistance. The characteristic features of GB MR are (i) a resistance drop by up to ∼33% accompanying the magnetization alignment of grains in moderate fields and (ii) an ongoing reduction in R in the Tesla range (up to 60 T [186]) (figure 11). The first has been called 'low-field MR' (LFMR) and the second 'high-field MR' (HFMR).

As pointed out by Hwang *et al* [187], the LFMR may originate from tunnelling of spin-polarized electrons through GBs, in analogy to tunnelling between ferromagnetic Ni grains in an insulating SiO_2 matrix ('granular MR') treated earlier by Helman and Abeles [188]. High-spin polarization of electrons

in metallic manganites results in large granular tunnelling MR. Note that direct tunnelling cannot account for the HFMR (assuming that the tunnel barrier itself is not altered by the field).

The LFMR seemed promising for versatile magnetic field sensors; hence, numerous types of GBs have been studied, e.g. single (artificial) GB in films grown on bicrystals [189–193], polycrystalline films [109, 119], sintered bulk ceramics (early work [187, 194, 195]), cold-pressed powder samples and step edge junctions [196]. Bicrystal experiments gave direct evidence of GB resistance by comparison (in a resistor bridge) of two stripe elements in a film, containing one or no GB. Unfortunately for applications, the temperature dependence of LFMR turned out to be severe, with LFMR $\leqslant 1\%$ at 300 K, even for bulk $T_C = 370$ K. Considering the close correlation of electron transfer and magnetic order in manganites, a *layer of reduced magnetic order around GB* was proposed. Balcells *et al* [195] have measured the reduced magnetization of grain surface layers in ceramics with low grain sizes (20–100 nm). In general, the disturbed GB layer has too low a volume fraction for detection of its magnetization contribution. The plan-view HRTEM of a bicrystal GB indicates the confinement of structural disorder to very few lattice constants [192]. Probably the best magnetic resolution of a GB has so far been achieved by MFM [150]. This experiment records an *increased* magnetization and T_C at a bicrystal GB in a $La_{0.7}Sr_{0.3}MnO_3/SrTiO_3$ film. This untypical behaviour originates from substrate-induced tensile stress in the film and its release near the GB [151], underlining the crucial role of mechanical strain. Since no really direct methods exist for the investigation of GB magnetism, most information so far has been derived from transport measurements.

6.1.1. Grain boundary transport models. All models assume the existence of a few nanometre wide layer around GBs with the magnetic structure deviating from that of the grains' interior, commonly treated as a magnetic phase with an ordering temperature and magnetization, M_{gb}. Models can be distinguished as follows: (i) electrons move between grains either by tunnelling or by (possibly activated) conduction. The latter case is considered in the mesoscopic MR model of Evetts *et al* [190]. (ii) Electron tunnelling may proceed directly [187] or via localized magnetic states inside the GB layer [191, 197]. Single GBs [191, 198] and step edge boundaries [196] show typical non-linear I–V characteristics. The voltage dependence of the conductance

$$G(V,T) = I/V = G_0(T) + G_\alpha(T)V^{\alpha(T)} \qquad (3)$$

with the temperature-dependent exponent α may indicate the dominating tunnelling process. For instance, $\alpha = 2$ for direct tunnelling at intermediate V [199, 200] and $\alpha = n - 2/(n+1)$ for tunnelling via n localized states, $n \geqslant 1$ [201, 191]. Paranjape *et al* [198] report $\alpha = 0.5$ attributed to tunnelling between disordered electrodes. (iii) The tunnel barrier (height, width) at GBs may depend on the magnetic field [193]. It might (partially) arise from an increased chemical potential for charge carriers due to the magnetic disorder [202]. One consequence of a chemical potential shift in the GB layer is a depletion of charge carriers [191]. Another consequence is a reduction of the tunnel barrier in large magnetic fields due to the increase in M_{gb} and, thus, large negative HFMR. (iv) With increasing temperature, spin–flip processes which involve the excitation of bulk or surface magnons might become important [203].

6.1.2. Magnetoconductance for tunnelling (assuming spin conservation)

Direct tunnelling. In a granular medium, the MR can be calculated from the spin polarization, P, and the magnetization, $m = M/M_\parallel$, (normalized to the value $M_\parallel$ for parallel spin orientation) like [204]

$$\frac{R(0) - R(H)}{R(H)} = \frac{G(H) - G(0)}{G(0)} = P^2 m^2 \leqslant 1. \qquad (4)$$

If the grains' magnetization vectors are randomly aligned at $H = 0$ (as assumed for equation (4)), the maximum reduction in R is 50% for $P = 1$. At very low temperature and for low grain size, tunnelling might be suppressed due to charging of grains, the *Coulomb blockade* effect. In this regime, simultaneous tunnelling of two electrons (one towards and one from the grain) may take place, the so-called *co-tunnelling* process that enhances the MR [203].

Indirect tunnelling via localized states in the barrier. According to a simple approach proposed by Lee *et al* [197], the tunnelling probability via a boundary state with spin $\boldsymbol{s}_b$ is (approximately) proportional to $(1 + \boldsymbol{s}_1 \cdot \boldsymbol{s}_b)(1 + \boldsymbol{s}_b \cdot \boldsymbol{s}_2)$, with $\boldsymbol{s}_1$, $\boldsymbol{s}_b$ and $\boldsymbol{s}_2$ denoting unit vectors parallel to the spins of the left electrode, the boundary state and the right electrode. In low fields, disordered grain boundary spins $\langle \boldsymbol{s}_b \rangle = 0$ ($M_{gb} = 0$) are assumed. The derived LFMR obtained at the saturation field H_S of the magnetization is

$$\frac{R(H=0) - R(H_S)}{R(H_S)} = \frac{G(H_S) - G(H=0)}{G(H=0)} = 1 + \frac{1}{3^n} m_S^2 \qquad (5)$$

for tunnelling via n boundary states ($n \geqslant 1$) [197, 205], with the normalized saturated sample magnetization, m_S. Note that the obtainable LFMR decreases with the number of tunnelling steps. The maximum value 4/3 obtained for $n = 1$ (only) roughly agrees with the experiments. In large fields $H > H_S$, conductance increases together with the GB magnetic order. With the normalized GB magnetization, m_{gb}, the conductance is estimated as

$$G_1 \propto 1 + \frac{1}{3} m_S^2 + 2 m_S m_{gb}(H) + \frac{2}{3} m_s^2 m_{gb}^2(H) \qquad (\text{for } n = 1). \qquad (6)$$

(For $n > 1$, see [205].) For small m_{gb} the last term vanishes, leaving $1/G(H = 0)\ \mathrm{d}G/\mathrm{d}H = 2 m_S \chi_{gb}$ [197] with the GB susceptibility, $\chi_{gb} = \mathrm{d}m_{gb}/\mathrm{d}H$. A mean-field calculation for the particular case of an antiferromagnetically ordered GB obtains another prefactor for χ_{gb} [206]. Hence, the particular case of linear $G(H)$ [186] is observed for $\chi_{gb} = \text{const}$ (and $m_{gb} \ll 1$).

6.2. Trilayer tunnel junctions

Reviews considering manganite tunnel structures are [18, 20, 130]. A well-defined tunnel barrier can be grown in epitaxial trilayer films comprising two conducting ferromagnetic manganite layers and a thin insulator (I) layer. First experiments concentrated on $La_{0.67}Sr_{0.33}MnO_3$ (LSMO)/$SrTiO_3$ (STO)/$La_{0.67}Sr_{0.33}MnO_3$ on $SrTiO_3$(100) substrates [15, 129, 130]. Standard photolithographic processes have been used to pattern *in situ* grown trilayers into junctions of several μm^2 in area. LSMO/STO/LSMO junctions revealed an extraordinary large low temperature tunnelling MR (TMR) with a resistance ratio of $R_{high}/R_{low} = 5$–20 at 4.2 K [15, 130, 207]. This might be the largest TMR known for any trilayer tunnel junction. Other investigated junctions are LSMO/$CaTiO_3$/LSMO [208], $La_{0.7}Ca_{0.3}MnO_3$ (LCMO)/$NdGaO_3$/$La_{0.7}Ca_{0.3}MnO_3$ [209, 210], LCMO/$La_{0.45}Ca_{0.55}MnO_3$/LCMO with an insulating manganite barrier [211], LSMO/TiO_2/LSMO [212] and LCMO/STO/$La_{0.7}Ce_{0.3}MnO_3$ [29]. Further barrier materials used are $LaAlO_3$, Al_2O_3 ([133] non-epitaxial), $Ce_{0.69}La_{0.31}O_{1.845}$ [213] and $PrBa_2Cu_3O_7$ [15].

Non-manganite second electrodes have been studied in LSMO/barrier/Co junctions [212–214] and LSMO/Al_2O_3/Permalloy junctions [215]. Worledge and Geballe [216] gave evidence of negative spin polarization of $SrRuO_3$ in LSMO/STO/$SrRuO_3$ junctions and tested the spin polarization of a LSMO/STO interface in a ferromagnet/I/superconductor junction using Al as superconductor [135]. Hu and Suzuki [217] found evidence of negative spin polarization of magnetite in Fe_3O_4/$CoCr_2O_4$/LSMO junctions.

Non-trilayer tunnel junctions may be formed wherever structural and magnetic disorder at surfaces or interfaces in manganites create a tunnel barrier. Besides GB, break junctions [218], piezoelectrically controlled pressure contacts between crystals [219] and nanoconstrictions of <100 nm width patterned into LSMO film stripes by focused ion beam milling [137] show tunnelling-like transport properties.

6.2.1. Models and mechanisms of spin-polarized tunnelling

The Jullière model. In 1975, Jullière proposed an expression for TMR in a trilayer made of two FM metals and an insulating barrier [10]. The tunnel conductance of an electron is proportional to the density of occupied states at the Fermi level (E_F) in the left electrode (prior to tunnelling) and the density of empty states in the right electrode (final state):

$$TMR = \frac{R_{\uparrow\downarrow} - R_{\uparrow\uparrow}}{R_{\uparrow\uparrow}} = \frac{G_{\uparrow\uparrow} - G_{\uparrow\downarrow}}{G_{\uparrow\downarrow}} = \frac{2P_1P_2}{1 - P_1P_2} \qquad (7)$$

with $R_{\uparrow\downarrow}(G_{\uparrow\downarrow})$ and $R_{\uparrow\uparrow}(G_{\uparrow\uparrow})$ denoting the resistance (conductance) for antiparallel and parallel orientation of the electrodes' magnetization vectors, respectively, and the spin polarizations P_1 and P_2 of the electrodes [10]. For $P_1 = P_2 \sim 1$ (half-metals), nominally unlimited values of TMR are achievable. Inverse TMR (i.e. TMR < 0) is observed if one of the electrodes has negative spin polarization. The Jullière model neglects any effect of (i) the tunnel barrier, (ii) the band structure of electrodes and (iii) spin–flip processes. Nevertheless, it rather successfully describes tunnelling data of many metal tunnel junctions, if the definition of spin polarization is modified appropriately (see below).

The generalized Jullière model. Equation (7) can be used to estimate the spin polarization from the measured TMR in a FM/I/FM junction at low temperature. Surprisingly, even the sign of P may depend on the barrier material. In a pioneering work in early 1970s, Meservey and Tedrow determined P of several metals (Co, Ni etc [220–222]) from current–voltage characteristics of FM/Al_2O_3/Al (Al superconducting) junctions and found $P > 0$ always. This result was in contrast to the higher minority band DOS at E_F in these metals, implying $P < 0$. De Teresa *et al* recorded inverse TMR for LSMO/STO/Co junctions but regular TMR for LSMO/Al_2O_3/Co, and proposed an interface-dependent polarization of electrons tunnelling from the Co electrode [213, 214]. While Al_2O_3/Co favours majority band s electrons for tunnelling, the $SrTiO_3$/Co interface seems to transmit minority band d electrons. A similar barrier-dependent TMR has been observed in NiFe/Ta_2O_5/AlO_x/NiFe layers [223]: the sign of TMR changes with the current direction. Thus, it is now accepted that it is not the ferromagnet's bulk properties but the ferromagnet-barrier interface which determines P of the tunnelling electrons. The LSMO/STO interface with its large positive spin polarization [135] is a useful 'spin analyser' to determine the spin polarization of another material (or correctly: material–STO interface) [217].

The direct influence of the *FM band structure* may be observed in tunnel junctions with sufficiently high tunnel barrier. The bias-dependent tunnel current will follow the integrated DOS according to

$$I = A \int_{-\infty}^{\infty} N_1\left(E + \frac{eV}{2}\right) N_2\left(E - \frac{eV}{2}\right) T(s, E, W) \left\{ f\left(E - \frac{eV}{2}\right) - f\left(E + \frac{eV}{2}\right) \right\} \mathrm{d}E \qquad (8)$$

with the DOS N_1 and N_2 of the FM electrodes, the transmission probability T depending on the barrier height W and width s, the Fermi-Dirac function f for the occupation probability of a state and the applied bias voltage V [224]. This effect is well known and utilized in scanning tunnelling spectroscopy (STS) measurements of DOS. An example of Co band structure details in bias-dependent TMR is found in [214].

6.2.2. Tunnelling MR. Tunnel trilayers have been structured into junctions of 1 μm^2 to 1 mm^2 in area. Single domain states of manganite electrodes can be obtained for a junction diameter of several micrometres [18, 210] (figure 12). Junctions containing a few FM domains show steps in $R(H)$ (figure 12(*c*)). The magnitude of the observed TMR is extremely large at low temperatures, with a resistance ratio of $R_{high}/R_{low} \sim 18$ for LSMO/STO/LSMO measured at 4.2 K (figure 12(*c*)) and $R_{high}/R_{low} \sim 7$ for $La_{0.7}Ca_{0.3}MnO_3$/$NdGaO_3$/LCMO measured at 77 K (figure 12(*b*)). This record TMR confirms the high spin polarization (the 'nearly' half-metallic nature) of the employed manganites. The in-plane angular dependence of magnetic switching fields of a single-domain state has been studied by the Cambridge group [225] in $La_{0.7}Ca_{0.3}MnO_3$/$NdGaO_3$/LCMO/NGO(001) junctions. It closely follows the ideal coherent rotation model.

Many manganite trilayer junctions show a high noise level in field-dependent resistance data. One reason for this

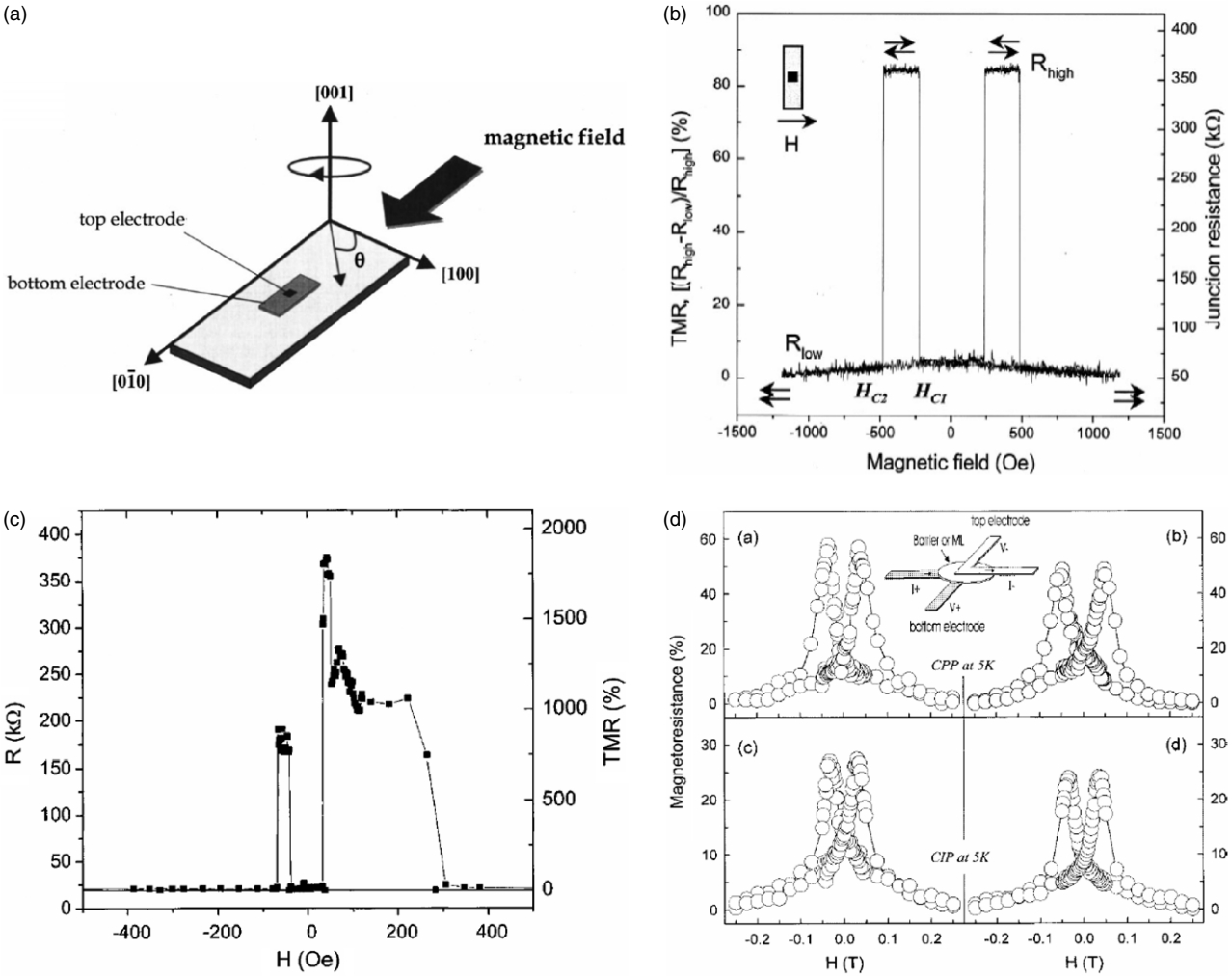

Figure 12. (*a*) Schematic structure of an epitaxial tunnel trilayer junction of $La_{0.7}Ca_{0.3}MnO_3/NdGaO_3/La_{0.7}Ca_{0.3}MnO_3$. The area of the top electrode is $6 \times 6\,\mu m^2$. (*b*) Tunnel resistance and magnetoresistance (TMR) of a junction from (*a*) measured at 77 K. (Both (*a*) and (*b*) adapted with permission from [209], ©2000 AIP.) (*c*) Record TMR measured on a $La_{0.67}Sr_{0.33}MnO_3/SrTiO_3/La_{0.67}Sr_{0.33}MnO_3$ junction at 4.2 K. Multistep switching indicates the presence of a few domains. (Reprinted with permission from [207], ©2003 AIP.) (*d*) Polycrystalline $La_{0.7}Ca_{0.3}MnO_3/Al_2O_3/La_{0.7}Ca_{0.3}MnO_3$ tunnel junction prepared using shadow masks (see geometry in the inset). Electrodes contain many magnetic domains in the junction area, leading to smooth curves without single switching events. (Reprinted with permission from [133], ©2000 AIP.)

might be an interaction of spin-polarized current with local magnetization leading to a current-dependent change in the magnetic domain distribution [226]. High local electric fields may even alter the phase of manganite clusters near the barrier from insulating to metal-like. Another unusual experimental finding is the light-induced change of the tunnel characteristics described by reduced barrier width under illumination [227].

6.2.3. Temperature dependence of TMR. The TMR, while being extremely large at low temperature, drops with increasing temperature much more quickly than the bulk magnetization [15, 129, 133, 169, 207, 210, 228]. Magnetic disorder at the manganite–barrier interface might be the origin of this behaviour (e.g. [174]). Garcia *et al* [228] found a less pronounced temperature dependence of the interface spin polarization (derived from TMR data and Jullière model) for some barrier materials if it is compared with that of a free surface (figure 13). Possibly, improved interface microstructure and an appropriate choice of barrier material might enhance the TMR achievable at 300 K. However, manganite TMR at ambient conditions is far below the large TMR known from Fe/MgO/Fe junctions [229].

7. Multiferroic manganite–titanate thin film systems

This paragraph concentrates on thin film systems comprising a FM manganite and a ferroelectric (FE) titanate. Manganite–titanate film systems have been studied for various reasons such as improved fatigue behaviour of titanate capacitors with manganite electrodes [230], ferroelectric field effect transistors (7.2) and the influence of piezoelectric strain on magnetic properties (7.3).

Composites of a FM and a FE compound (called bi- or multiferroic) have been investigated with increasing interest for several years, since they are favourable candidates for the observation of strong magnetoelectric phenomena [162].

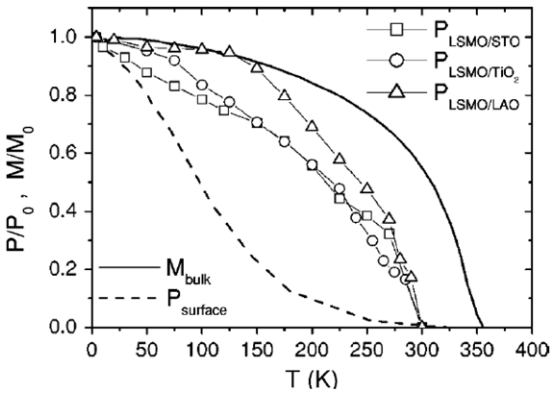

Figure 13. Temperature dependence of the normalized spin polarization at the interface between $La_{0.67}Sr_{0.33}MnO_3$ and three different insulators, $SrTiO_3$, TiO2 and $LaAlO_3$, as derived from tunnel magnetoresistance measurements and the Julliere model (see text). Normalized bulk magnetization and spin polarization of a free $La_{0.7}Sr_{0.3}MnO_3$ surface as measured by spin-polarized photoelectron spectroscopy are shown for comparison. (Reprinted with permission from [228], ©2004 APS.)

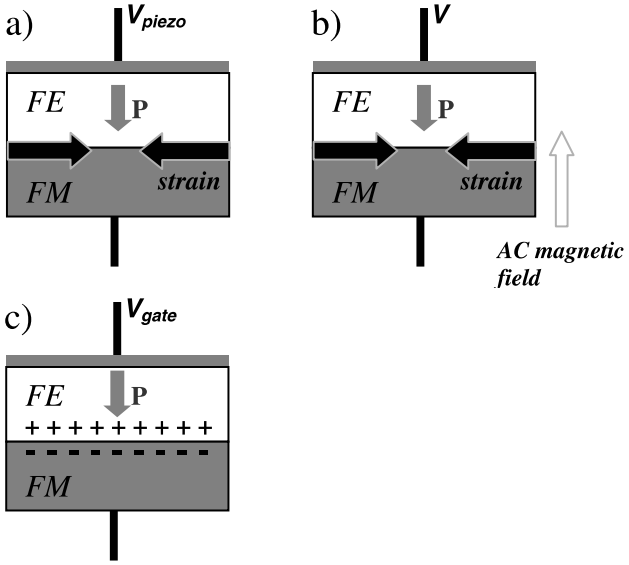

Figure 14. Schematic illustration of a ferroelectric (FE)—ferromagnetic (FM) bilayer and its coupling mechanisms. (*a*) Application of an electric voltage (V_{piezo}) to the FE layer causes the inverse piezoelectric strain to be transferred to the magnetic layer. This effect can be utilized for the control of strain-dependent magnetic properties. (*b*) Application of a magnetic ac field causes strain by magnetostriction coupled into the FE layer. The induced piezovoltage is particularly large for certain electromechanical resonance frequencies. (*c*) Polarization (P) of the FE layer is associated with surface charges at the FE / FM interface and an electric stray field into the FM layer resulting in an interface-near charge depletion or accumulation (electric field effect).

The magnetoelectric effect describes the phenomenon when magnetization is induced by an electric field (E), or an electric polarization (P_E) is induced in a magnetic field. This behaviour is expressed by a term αEH in the free energy of a material, with the magnetoelectric tensor α. A review on magnetoelectric phenomena in compounds and composites can be found in [162]. The interrelation of magnetic and ferro- / dielectric properties is clearly promising from a technological perspective, since new functionalities might arise. For instance, electric control of magnetization might open new ways for magnetic data storage/recording and electromagnetic transducers.

Very few compounds are intrinsically (anti)ferromagnetic and ferroelectric [231,232]. Even if both ferroic properties are present, coupling between the two order parameters may be weak. Strong magnetoelectric effects are found, for instance, in hexagonal $HoMnO_3$ [233], in perovskite $RMnO_3$ for R = Tb; Dy [234, 235], in RMn_2O_5 (R = Dy [236], Tb [237]), $BiMnO_3$ [238] and in a spinel sulfide, $CdCr_2S_4$ [239]. Most multiferroic compounds known so far have restrictions for practical utilization: (i) the magnetoelectric properties are observed below 100 K and (ii) P_E or M are much smaller than in conventional ferromagnets or ferroelectrica. *Composites* of FM and FE compounds are favourable regarding these aspects: they can be chosen with high transition temperatures and polarizations.

7.1. Mechanisms of magnetoelectric coupling in layered composites

A bilayer of a FM and a FE film is considered (figure 14). The two layers can influence each other via (i) mechanical stress and (ii) electric or magnetic stray fields.

Inverse piezoelectric effect. An electric voltage applied to the FE component will stretch the full bilayer due to the inverse piezoelectric effect (figure 14(*a*)). (We assume magnetic layer is conducting; hence it can serve as an electrode.) Mechanical coupling between the layers determines the efficiency of strain mediation to the magnetic layer. In epitaxially grown films, generally good mechanical coupling can be anticipated, depending on interface roughness / lattice defects. Manganites as well as other 3d TM oxides are particularly sensitive to biaxial deformation of the crystal lattice [27, 178, 240]. Epitaxial strain in thin films shifts T_C, modifies magnetic anisotropy [181–183] and might even induce metal-insulator phase transitions [176]. The general reason for the strong strain sensitivity is the presence of competing interactions that depend on crystallographic bond angles and lengths. It seems likely that magnetic properties of some TM oxides might be controllable to a significant extent by strain in bilayer systems.

(Direct) magnetoelectric effect (figure 14(b)). When an alternating magnetic field is applied to the bilayer stack (or a multilayer of piezoelectric and magnetostrictive films), mechanical strain arises from the magnetostriction of the FM component. It induces, again dependent on mechanical interlayer coupling, a piezovoltage in the FE component. The frequency-dependent magnetoelectric coefficient $\alpha(\omega)$ is defined as voltage per magnetic field and height of the sample stack. Longitudinal and transverse α are distinguished for orientations of applied H and measured E (i.e. voltage) perpendicular or parallel to each other, respectively. Maxima of α can be obtained at electromechanical resonance frequencies [241–243].

Electric field effect (figure 14(c)). A ferroelectric polarization creates a surface charge density at the FE–FM interface. The resulting electric field in the magnet is screened by an

equal number of charge carriers of opposite sign. For this classical field effect to appear, a dielectric layer is sufficient. Additionally, the hysteresis of $P_E(E)$ allows hysteretical charge carrier modulation with remanent states. The change in charge carrier density per surface area of the ferroelectric layer is $\Delta\sigma = P/e$ (with elementary charge e). Assuming $P = 35\,\mu C\,cm^{-2}$, 0.5 electrons per unit cell could be controlled in a magnetic film being one unit cell (4 Å) thick.

7.2. Field effect devices

The field effect in oxides has been adressed by Ahn *et al* [244]. Historically, first experiments on manganite–titanate epitaxial films were done on typical field effect transistor (FET) structures [245–248]. It was understood later (proposed by Ogale *et al* [245] and Tabata *et al* [247], demonstrated recently by Thiele *et al* [136]) that piezoelectric strain might additionally influence the observed resistance modulations.

The field effect is observable with a dielectric gate electrode ($SrTiO_3$), as in the early experiment reported by Ogale *et al* [245]. This work finds a shift in T_{MI} of $Nd_{0.7}Sr_{0.3}MnO_3$ by a few Kelvin and an R modulation of several per cent for an electric field of $E \sim 50\,kV\,cm^{-1}$. Here and in some other publications, the response of R to an electric field is called 'electroresistance' (in analogy to MR). Interestingly, the field effect did not show a clear dependence on the sign of the applied voltage but appeared to depend rather quadratically on gate voltage leading to the proposal of a strain effect. In 1997, a huge hysteretic ΔR of ~300% at 300 K has been reported for another all-oxide FET of $Pt/PbZr_{0.2}Ti_{0.8}MnO_3/La_{0.7}Ca_{0.3}MnO_3/LaAlO_3$ where a FE gate layer of $PbZr_{0.2}Ti_{0.8}MnO_3$ (PZT) was employed [246]. The remanent states had a retention loss of few per cent within an hour, indicating potential as non-volatile multiferroic memory. In 2001, Wu *et al* [248] reported on another observation of large R modulation (up to 100% at 300 K); their FET device had a different stacking sequence (FM/FE/substrate) using a conducting substrate, $La_{0.7}Ca_{0.3}MnO_3$(50 nm)/$PbZr_{0.2}Ti_{0.8}O_3$/Nb(1at%):$SrTiO_3$ (100). Further manganite channels ($Nd_{0.7}Sr_{0.3}MnO_3$, $La_{0.7}Ba_{0.3}MnO_3$ and $La_{0.5}Ca_{0.5}MnO_3$) showed lower R modulation of few per cent [248], even for half-doped $La_{0.5}Ca_{0.5}MnO_3$, that is near a metal-insulator phase boundary according to the bulk phase diagram (figure 4). Other unexpected results were the unchanged T_{MI} and strong R modulation in a *thick* (50 nm) $La_{0.7}Ca_{0.3}MnO_3$ channel layer. Assuming a nominal carrier density of 0.3 per unit cell, the electric field is screened within few unit cells, leaving the remaining channel unchanged. Wu *et al* proposed a phase-separated metal/insulator cluster state that changes with respect to volume fractions of the phases under electric field [248]. This might also leave T_{MI} at constant temperature.

Later experiments [136, 249–252] have found R modulations of smaller magnitude. Kanki *et al* [250] investigated FET structures of $Au/PbZr_{0.2}Ti_{0.8}O_3/La_{1-x}Ba_xMnO_3/SrTiO_3(100)$ ($x = 0.1$; 0.15) (figure 15) with narrow manganite layers (6 nm) prepared by pulsed laser deposition. They report complete hysteresis loops of channel resistance versus gate voltage and demonstrate their commensurate nature with ferroelectric

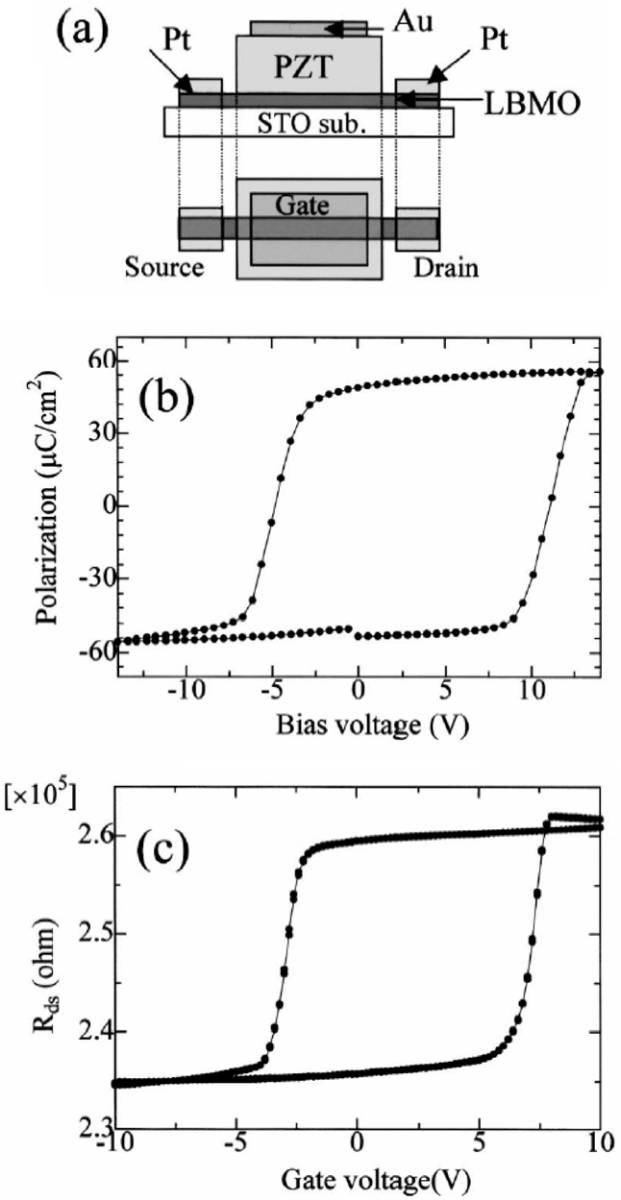

Figure 15. (*a*) Geometry of a $PbZr_{0.2}Ti_{0.8}O_3$/$La_{0.9}Ba_{0.1}MnO_3$(6 nm)/$SrTiO_3$ field effect device. (*b*) Gate polarization (P) loop versus gate voltage and (*c*) channel resistance (R) loop versus gate voltage measured at 300 K indicate that R changes proportional to P. (Reprinted with permission from [250], ©2003 AIP.)

polarization. The resistance modulation has been estimated as

$$\frac{\Delta R}{R} = \frac{\Delta n}{n} = \frac{P_E}{edn} \tag{9}$$

with the (volume) carrier density n, elementary charge e and channel width d. Equation (9) indicates that low doping (low n) and low d enhances $\Delta R/R$. Of course equation (9) is a rather simple approximation, assuming (i) constant mobility of charge carriers within the range $n \pm \Delta n$ and (ii) homogeneous distribution of Δn throughout the channel width d. Nevertheless, it is in agreement with the order of ΔR observed in some recent experiments [249–251], such as $\Delta R/R = 10\%$ for $La_{0.9}Ba_{0.1}MnO_3$ at 300 K. Further,

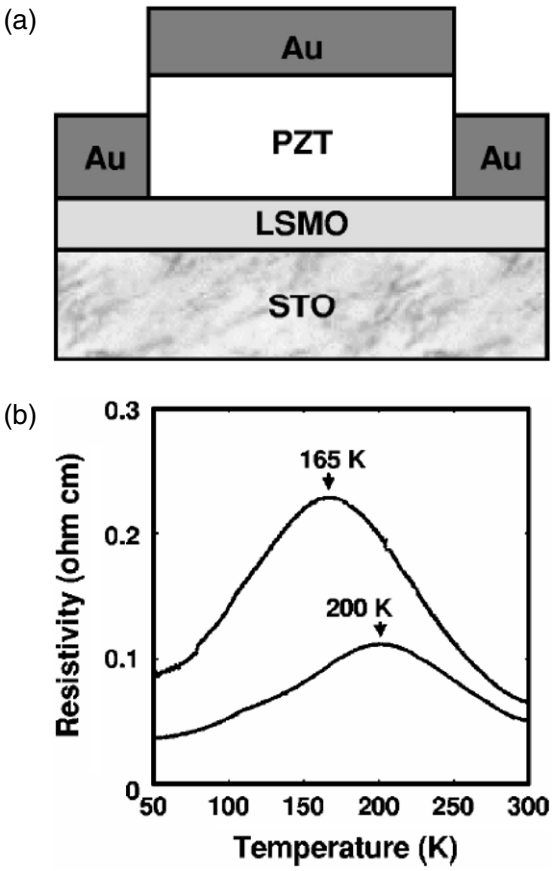

Figure 16. (*a*) Schematic device structure of a $PbZr_xTi_{1-x}O_3$/$La_{0.8}Sr_{0.2}MnO_3$ field effect device. (*b*) Resistivity as a function of temperature for the two states of remanent polarization of the PZT gate layer. The upper curve belongs to the hole depletion state, the lower to the hole accumulation state. (Adapted with permission from [249], ©2003 APS.)

an approximately linear increase in ΔR with P_E has been found [250]. Hong *et al* [249] investigated a FET structure of Au/PZT/$La_{0.8}Sr_{0.2}MnO_3$(4 nm)/$SrTiO_3$ and obtained a room temperature resistance ratio of 1.28. Figure 16 reproduces the temperature dependence of R for their device at positive and negative remanent polarization of the PZT layer. Here, the shift in T_{MI} is consistent with the reduced (increased) carrier density for positive (negative) gate voltage. Zhao *et al* [251] reported on a FET device with a $La_{0.8}Ca_{0.2}MnO_3$ channel grown on Si (using $SrTiO_3$/Si epitaxy). This work finds a maximum $\Delta R/R \sim 20\%$ slightly below $T_{MI} \sim 200$ K, while $\Delta R/R$ at 300 K is small (~2%). In general, the observed field effect in manganites depends on temperature. Thus, the systematics of field effect in manganites (dependence on chemical composition, terminations at the manganite-titanate interface, temperature and magnetic field) are yet to be explored.

7.3. Strain control of magnetic properties

The controlled deformation of the crystal lattice is very useful to explore the influence of structure on magnetic properties for any crystalline material. Besides hydrostatic pressure, an epitaxial strain of thin films grown on slightly mismatching single-crystal substrates is regularly applied for this purpose. While most work utilizes substrates with slightly larger or lower lattice constants, it seems promising to exploit the inverse piezoelectric effect of a FE buffer layer or substrate for continuous control of lattice parameters by the application of electric voltage.

Several oxide ferroelectrics with good piezoelectric properties have a perovskite-like lattice with similar pseudocubic lattice parameter (~4 Å) such as FM manganites. Examples are $BaTiO_3$ (BTO), $PbZr_{1-x}Ti_xO_3$ (PZT), and $Pb(Mg_{1/3}Nb_{2/3})_{1-x}Ti_xO_3$ (PMN-PT). Tabata and Kawai proposed that the piezoelectric strain may contribute to the R modulation in a FET structure [247]. Indeed, while a massive substrate suppresses the piezoelectric strain of a thin film, it may show a minor strain effect. If only the regular field effect ($\Delta R \propto P_E$) and the strain effect are present it was proposed to distinguish both contributions considering the shape (square-shaped, as in figure 15, or butterfly-like, as in figure 17) of R hysteresis loops [136].

Strong mechanical coupling to a substrate diminishes the strain achievable in the film plane. Two ways have been proposed to overcome this problem: (i) piezoelectric substrates [121, 253, 254] figure 17 and (ii) columnar nanostructures where columns can expand perpendicular to the substrate plane [255].

Concerning the first approach, $BaTiO_3$ crystals [253, 254] and PMN-PT(001) crystals [121] have been studied. Structural phase transitions of $BaTiO_3$ at ~290 K and at ~190 K were allowed to record the accompanying R and M changes in $La_{0.67}Sr_{0.33}MnO_3$ and $SrRuO_3$ films [253]. In the LSMO 50 nm film, large jumps (70%) of the low-field ($H = 20$ Oe) magnetization at substrate structural transitions and substantially modified $M(H)$ loops indicating a changed magnetic anisotropy have been detected. R increases by about 12% at 290 K due to an increase in (anisotropic) in-plane strain by ~0.21%. The influence of varied epitaxial strain at structural transitions on R and M in $La_{0.5}Sr_{0.5}MnO_3$/$BaTiO_3$(001) is investigated similarly [254]. Further, in this work film strain is also tuned by a voltage applied to the BTO crystal. An R reduction of about 12% at 300 K in a 50 nm thick film has been found for $E \sim 1$ kV cm^{-1} in the crystal and is attributed to reduced in-plane strain of the film. ($BaTiO_3$ has a larger lattice parameter than $La_{0.5}Sr_{0.5}MnO_3$ and contracts in the film plane under electric field applied along [001].) Time-dependent R data show relaxation within several hours attributed to slow polarization dynamics of the $BaTiO_3$ crystal [254]. Since twinned BTO causes non-uniform in-plane strain in an epitaxially grown film, the quantitative analysis of strain-dependent R/M behaviour of the film is difficult. Another piezoelectric single-crystal substrate material might be advantageous: PMN-PT(001) with a pseudocubic lattice parameter of ~4.02 Å seems capable of quick and reversible control of in-plane strain states associated with less inhomogeneity of local in-plane strain [121]. For epitaxial films of $La_{0.7}Sr_{0.3}MnO_3$/PMN–PT(001), strain-induced reversible R and M modulations at ambient temperature (figure 17) and strain-dependent T_C have been recorded for an in-plane strain level up to ~0.15%. Indeed, PMN-PT(001) crystals would allow the application of much larger in-plane strain up to above 1% [256]. The limiting factors of the recent experiment [121] were the voltage needed

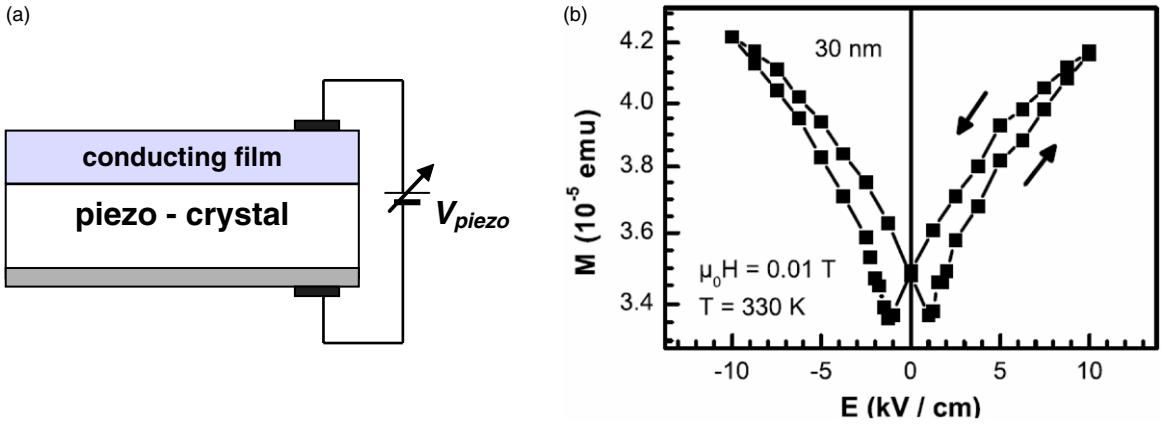

Figure 17. (*a*) Principle of dynamic biaxial strain control in a thin film on a piezoelectric substrate. In the case of a conducting film, the voltage is applied to the substrate crystal using a metal bottom electrode and the film itself. Insulating films require a conducting (epitaxial) buffer layer between substrate and film as top electrode. (*b*) (Courtesy of C Thiele.) Magnetization modulation of a $La_{0.7}Sr_{0.3}MnO_3/Pb(Mg_{1/3}Nb_{2/3})_{0.72}Ti_{0.28}O_3(001)$ film induced by piezoelectric strain. The electric field is applied along [001] (the substrate normal), the magnetic field along [100] in the film plane (referring to pseudocubic lattice). (Courtesy of C Thiele.)

to achieve $E > 10\,\mathrm{kV\,cm^{-1}}$ and the avoidance of dielectric breakthrough and arcing.

Along the way (ii) out of the substrate 'clamping problem', $BaTiO_3$–$CoFe_2O_4$ nanocolumnar films on $SrTiO_3(001)$ substrates have been investigated by Zheng *et al* [255]. A mixed target of both components was used for PLD. The films grew in a self-assembled structure with $CoFe_2O_4$ nanopillars (of diameter 20–30 nm) embedded in a $BaTiO_3$ matrix. They showed large room temperature values of spontaneous magnetization and ferroelectric polarization and a jump of M at the ferroelectric Curie temperature $T_{CE} \sim 390\,\mathrm{K}$. The latter is a demonstration of magnetoelectric coupling attributed to the elastic interaction between the components. The spinel is an insulator; thus, the electric field can be applied along the long axis of the nanopillars. (For conducting ferromagnets such as manganites, only in-plane electric fields would be possible for such nanocolumnar structures.) If this method of self-assembly would not work for the desired components, nanocomposites could be prepared using, for instance, a colloidal templating method. Kim *et al* [257] covered a substrate with a suspension of polymethyl methacrylate (PMMA) spheres (of 400 nm in diameter, but smaller ones are possible) in a $La_{0.7}Ca_{0.3}MnO_3$ precursor solution. The PMMA spheres form a regular hexagonal lattice and produce pores in the reacted manganite. These pores have been filled with $BaTiO_3$ solution dried and reacted afterwards.

8. Conclusions

8.1. Summary

Publications on perovskite manganites are numerous, exceeding one thousand per year since 1998. Recently, saturation and slight decay of activities have been reached. This review intends to present some main routes of research and collects characteristic features of magnetic and electric/electronic properties of ferromagnetic manganites, including related magnetic phases. The microscopic mechanisms dominating electronic and magnetic behaviour have been described in a phenomenological framework. Magnetic phase diagrams are governed by three fundamental chemical parameters which are (i) the doping level, (ii) the electronic band width governed by average ionic radii on metal sites in the lattice and (iii) the degree of disorder (variance of ionic radii at both metal sites). They reveal close neighbourhood (with respect to the ground state total energy) or even coexistence of (i) charge and orbital ordered antiferromagnetic insulating, (ii) ferromagnetic spin-polarized conducting and (iii) insulating SG-like phases. Ferromagnetic low-temperature properties are characterized by low magnetic anisotropy (if not modified by substitution of certain rare earth elements), leading to strong impact of stress-induced anisotropy in films. The critical behaviour has been found to be unconventional for some ferromagnetic manganites and seems to be strongly related to disorder. Multicriticality is one of the discussed origins of CMR. A higher degree of disorder, as obtained, for instance, by substitution of other TMs on Mn lattice sites, changes the magnetic state from ferromagnetic to spin or cluster glass-like. Electric transport in single crystals and polycrystalline samples is fundamentally different, the latter resembling granular ferromagnets. This is due to large additional resistance contributions from magnetically less ordered grain boundaries. Spin-polarized tunnelling in $La_{0.7}A_{0.3}MnO_3$ (A = Sr; Ca) shows record effects at 4.2 K being useful for the analysis of spin polarization of other materials ('spin analyser'). However, the strong temperature-dependent decay of tunnelling MR attributed tentatively to suppressed ferromagnetic order at interfaces destroys any chance of application at ambient conditions. Layered heteroepitaxial film systems of ferromagnetic manganites and ferroelectric titanates are investigated in an upcoming research area related to multiferroicity and magnetoelectric phenomena in composite materials. They appear particularly promising for biaxial strain control of magnetic properties in thin films, and further show a hysteretic polarization-induced electric field effect at the ferromagnetic–ferroelectric interfaces.

8.2. Outlook

About twelve years after the preparation of the first films of ferromagnetic spin-polarized manganites, commercial

relevance is not yet achieved for this class of materials. Instead, the process of discovery of new phenomena related to phase competition and enhanced sensitivity to many external parameters (magnetic and electric fields, light, lattice deformations etc) is going on. Whether this situation will change in the near future is hard to predict. While phase diagrams have been revealed for bulk compounds in recent years, there is still a lack of systematic studies on surface and interface properties (addressing, for instance, interface electronic structure).

It seems rather unlikely that manganites or other half-metal-like TM oxides might replace metals such as Co, Fe, Ni or their alloys in 'conventional' spin-polarized devices like trilayer tunnel junctions for MRAMs. The low ferromagnetic transition temperature ($\leqslant$370 K) and altered properties of surfaces/interfaces due to the competition of energetically neighbouring phases and complex chemical composition in manganites have turned out to be two major obstacles. Similarly, semiconductor-derived microelectronic functional structures such as field effect devices with manganite channels or manganite-based diodes are only of fundamental interest so far; they are inferior to respective doped semiconductor structures. Possibly, new concepts for functional devices *based on the specifics of strongly correlated TM oxides* might evolve in future. This might include the utilization of the inherent strong strain sensitivity of magnetic and electronic properties or field- or light-induced modification of charge and orbital ordered patterns since these can persist up to higher temperatures, e.g. about 600 K in Bi manganites, than the ferromagnetic order.

Acknowledgments

I am thankful to my colleagues at IFW Dresden, in particular to K-H Müller, for valuable discussions and joint experiments, and to L Schultz for continuous support of my work. Furthermore, I would like to thank all those colleagues in Germany and abroad for their advice, cooperation and fruitful exchange of ideas.

Financial support by Deutsche Forschungsgemeinschaft (DFG) during recent years in the framework of the Sonderforschungsbereich SFB 422 and the Research Group 520 Ferroic Functional Elements is gratefully acknowledged.

Reproduction of figures has been done with the permission of the publisher and, where possible, at least one of the authors.

References

[1] Jonker G H and van Santen J 1950 *Physica* **16** 337
[2] Jonker G H and van Santen J 1950 *Physica* **16** 599
[3] Volger J 1954 *Physica* **20** 49
[4] Zener C 1951 *Phys. Rev.* **82** 403
Zener C 1951 *Phys. Rev.* B **81** 440
[5] Pollert E, Krupicka S and Kuzwicova E 1982 *J. Phys. Chem. Solids* **43** 1137
[6] Opik U and Pryce M H L 1957 *Proc. R. Soc. Lond. Ser. A—Math. Phys. Sci.* **238** 425
[7] von Helmolt R, Wecker J, Holzapfel B, Schultz L and Samwer K 1993 *Phys. Rev. Lett.* **71** 2331
[8] Baibich M N, Broto J M, Fert A, Nguyen Van Dau F, Petroff F, Etienne P, Creuzet G, Friedrich A and Chazelas J 1988 *Phys. Rev. Lett.* **61** 2472
[9] Grünberg P, Schreiber R, Pang Y, Brodsky M B and Sowers H 1986 *Phys. Rev. Lett.* **57** 2442
[10] Julliere M 1975 *Phys. Lett.* **54A** 225
[11] Monsma D J, Lodder J C, Popma Th J A and Dieny B 1995 *Phys. Rev. Lett.* **74** 5260
[12] Dijken S van, Jiang X and Parkin S S P 2003 *Appl. Phys. Lett.* **83** 951
[13] Ohno Y, Young D K, Beschoten B, Matsukura F, Ohno H and Awschalom D D 1999 *Nature* **402** 790
[14] Lezaic M, Galanakis I, Bihlmayer G and Blügel S 2005 *J. Phys. Cond. Mat.* **17** 3121
[15] Viret M, Drouet M, Nassar J, Contour J P, Fermon C and Fert A 1997 *Europhys. Lett.* **39** 545
[16] Venkatesan M, Velasco P, Alonso J A, Martínez J L and Coey J M D 2004 *J. Phys.: Condens. Matter* **16** 3465
[17] Dietl T 2003 *Nature Mater.* **2** 646
[18] Ziese M 2002 *Rep. Prog. Phys.* **65** 143
[19] Goldschmidt V 1958 *Geochemistry* (Oxford: Oxford University Press)
[20] Coey J M D, Viret M and von Molnár S 1999 *Adv. Phys.* **48** 167
[21] Dagotto E, Hotta T and Moreo A 2001 *Phys. Rep.* **344** 1
[22] Daoud-Aladine A, Rodríguez-Carvajal J, Pinsard-Gaudart L, Fernández-Díaz and Revcolevschi A 2002 *Phys. Rev. Lett.* **89** 097205
[23] Coey M 2004 *Nature* **430** 155
[24] Anderson P W and Hasegawa H 1955 *Phys. Rev.* **100** 675
[25] Goodenough J B 1955 *Phys. Rev.* **100** 564
[26] Atanasov M and Angelov S 1991 *Chem. Phys.* **150** 383
[27] Millis A J 1998 *Nature* **392** 147
[28] Burns R G 1992 *Mineralogical Applications of Crystal Field Theory* 2nd edn (Cambridge: Cambridge University Press)
[29] Mitra C, Raychaudhuri P, Dörr K, Müller K-H, Schultz L, Oppeneer P M and Wirth S 2003 *Phys. Rev. Lett.* **90** 017202
[30] Gor'kov L P and Kresin V Z 2004 *Phys. Rep.* **400** 149
[31] Radaelli P G, Iannone G, Marezio M, Hwang H Y, Cheong S-W, Jorgensen J D and Argyriou D N 1997 *Phys. Rev.* B **56** 8265
[32] Ibarra M R and De Teresa J M 1999 *Giant Magnetoresistance and Related Properties of Metal Oxides* ed C N R Rao and B Raveau (Singapore: World Scientific) pp 83–155
[33] Tomioka Y and Tokura Y 2004 *Phys. Rev.* B **70** 014432
[34] Wollan E O and Koehler W C 1955 *Phys. Rev.* **100** 545
[35] De Gennes P-G 1960 *Phys. Rev.* **118** 141
[36] Ahn K H, Lookman T and Bishop A R 2004 *Nature* **428** 401
[37] Savosta M M, Karnachev A S, Krupicka S, Hejtmánek J, Jirák Z, Marysko M and Novák P 2000 *Phys. Rev.* B **62** 545
[38] Allodi G, De Renzi R, Guidi G, Licci F and Pieper M W 1997 *Phys. Rev.* B **56** 6036
[39] Fäth M, Freisem S, Menovsky A A, Tomioka Y, Aarts J and Mydosh J A 1999 *Science* **285** 1540
[40] Becker T, Streng C, Luo Y, Moshnyaga V, Damaschke B, Shannon N and Samwer K 2002 *Phys. Rev. Lett.* **89** 237203
[41] Renner C, Aeppli G, Kim B G, Soh Y A and Cheong S-W 2002 *Nature* **416** 518
[42] Uehara M, Mori S, Chen C H and Cheong S-W 1999 *Nature* **399** 560
[43] Murakami Y, Yoo J H, Atou T and Kikuchi M 2003 *Nature* **423** 965
[44] Loudon J C, Mathur N D and Midgley P A 2002 *Nature* **420** 797
[45] Fiebig M, Miyano K, Tomioka Y and Tokura Y 1998 *Science* **280** 1925
[46] Raquet B, Anane A, Wirth S, Xiong P and von Molnár S 2000 *Phys. Rev. Lett.* **84** 4485
[47] Hess F M, Merithew R D, Weissman, Tokura Y and Tomioka 2001 *Phys. Rev.* B **63** 180408
[48] Podzorov V, Uehara M, Gershenson M E, Koo T Y and Cheong S W 2000 *Phys. Rev.* B **61** R3784

[49] Saurel D, Mercone S, Guiblin N, Hardy V, Brûlet A, Martin C and Simon Ch 2004 *Physica* B **350** 51
[50] Viret M, Ott F, Renard J P, Glättli H, Pinsard-Gaudart L and Revcolevschi A 2004 *Phys. Rev. Lett.* **93** 217402
[51] Tokura Y, Tomioka Y, Kuwahara H, Asamitsu A, Moritomo Y and Kasai M 1996 *J. Appl. Phys.* **79** 5288
[52] Asamitsu A, Tomioka Y, Kuwahara H and Tokura Y 1997 *Nature* **388** 50
[53] Kiryukhin V , Casa D , Hill J P , Keimer B , Vigliante A , Tomioka Y and Tokura Y 1997 *Nature* **386** 813
[54] Takeshita N, Terakura C, Akahoshi D, Tokura Y and Takagi H 2004 *Phys. Rev.* B **69** R180405
[55] Zhang J, Tanaka H, Kanki T, Choi J H and Kawai T 2001 *Phys. Rev.* B **64** 184404
[56] Kirste A, Goiran M, Respaud M, Vanaken J, Broto J M, Rakoto H, Ortenberg M von, Frontera C and Garcia-Muñoz J L 2003 *Phys. Rev.* B **67** 134413
[57] Sahana M, Rössler U K, Ghosh N, Elizabeth S, Bhat H L, Dörr K, Eckert D, Wolf M, Müller K-H 2003 *Phys. Rev.* B **68** 144408
[58] Kim D, Revaz B, Zink B L, Hellman F, Rhyne J J and Mitchell J F 2002 *Phys. Rev. Lett.* **89** 227202
[59] Mira J, Rivas J, Hueso L E, Rivadulla F, López Quintela M A, Señaris Rodriguez M A and Ramos C A 2001 *Phys Rev* B **65** 024418
[60] Rößler S, Rößler U K, Nenkov K, Eckert D, Yusuf S M, Dörr K and Müller K-H 2004 *Phys. Rev.* B **70** 104417
[61] Salamon M B, Lin P and Chun S H 2002 *Phys. Rev. Lett.* **88** 197203
[62] Uhlenbruck S *et al* 1999 *Phys. Rev. Lett.* **82** 185
[63] Sahana M, Dörr K, Doerr M, Eckert D, Müller K-H, Nenkov K, Schultz L and Hegde M S 2000 *J. Magn. Magn. Mater.* **213** 253
[64] Smolyaninova V N, Hamilton J J, Greene R L, Mukovskii Y M, Karabashev S G and Balbashov A M 1997 *Phys. Rev.* B **55** 5640
[65] Ghosh N, Elizabeth S, Bhat H L, Rößler U K, Nenkov K, Rößler S , Dörr K and Müller K H 2004 *Phys. Rev.* B **70** 184436
[66] Schwarz A, Liebmann M, Kaiser U, Wiesendanger R, Noh T W and Kim D W 2004 *Phys. Rev. Lett.* **92** 077206
[67] Mydosh J A 1993 *Spin Glasses: An Experimental Introduction* (London: Taylor and Francis)
[68] Tomioka Y and Tokura Y 2004 *Phys. Rev.* B **70** 014432
[69] Akahoshi D, Uchida M, Tomioka Y, Arima T, Matsui T and Tokura Y 2003 *Phys. Rev. Lett.* **90** 177203
[70] Cai J-W, Wang C, Shen B-G, Than J-G and Zhan W-S 1997 *Appl. Phys. Lett.* **71** 1727
[71] Simopoulos A, Pissas M, Kallias G, Devlin E, Moutis N, Panagiotopoulos I, Niarchos D, Christides C and Sonntag R 1999 *Phys. Rev.* B **59** 1263
[72] Manoharan S S , Sahu R K , Rao M L , Elefant D and Schneider C M 2002 *Europhys. Lett.* **59** 451
[73] Alonso J L, Fernandez L A, Guinea F, Laliena V and Martín-Mayor V 2002 *Phys. Rev.* B **66** 104430
[74] Yusuf S M, Sahana M, Hegde M S, Dörr K and Müller K-H 2000 *Phys. Rev.* B **62** 1118
[75] Lakshmi S L, Dörr K, Nenkov K, Sridharan V, Sankara Sastry V and Müller K-H 2005 *J. Magn. Magn. Mater.* **290** 924
[76] Deac I G, Mitchell J F and Schiffer P 2001 *Phys. Rev.* B **63** 172408
[77] De Teresa J M, Ibarra M R, Algarabel P A, Ritter C, Marquina C, Blasco J, Garcia J, del Moral A and Arnold Z 1997 *Nature* **386** 256
[78] Lottermoser T, Fiebig M, Fröhlich D, Leute St and Kohn K 2001 *J. Magn. Magn. Mater.* **226** 1131
[79] Troyanchuk I O, Khalyavin D D, Trukhanov S V and Szymczak H 1999 *J. Phys.: Condens. Matter* **11** 8707
[80] Bartolomé F, Bartolomé J and Campo J 2002 *Physica* B **312** 769
[81] Dupont F, Millange F, de Brion S, Janossy A, Chouteau G 2001 *Phys. Rev.* B **64** 220403
[82] Wu S Y, Kuo C M, Wang H Y, Li W-H, Lee K C, Lynn J W and Liu R S 2000 *J. Appl. Phys.* **87** 5822
[83] Muñoz A, Alonso J A, Martínez M J, Garcia-Muñoz J L and Fernández-Diaz 2000 *J. Phys.: Condens. Matter* **12** 1361
[84] Hemberger J, Brando M, Wehn R, Ivanov V Yu, Mukhin A A, Balbashov A M and Loidl A 2004 *Phys. Rev.* B **69** 064418
[85] López J, de Lima O F, Lisboa-Filho P N and Araujo-Moreira F M 2002 *Phys. Rev.* B **66** 214402
[86] Wahl A, Hardy V, Martin C and Simon Ch 2002 *Eur. Phys. J.* B **26** 135
[87] Worledge D C, Jeffrey Snyder G, Beasley M R and Geballe T H 1996 *J. Appl. Phys.* **80** 5158
[88] De Teresa J M, Dörr K, Müller K H, Schultz L and Chakalova R I 1998 *Phys. Rev.* B **58** R5928
[89] Viret M, Ranno L and Coey J M D 1997 *Phys. Rev.* B **55** 8067
[90] Wagner P, Gordon I, Trappeniers L, Vanacken J, Herlach F, Moshchalkov V V, Bruynseraede Y 1998 *Phys. Rev. Lett.* **81** 3980
[91] Urushibara A, Morimoto Y, Arima T, Asamitsu A, Kido G and Tokura Y 1995 *Phys. Rev.* B **51** 14103
[92] Hundley M F, Hawley M, Heffner R H, Jia Q X, Neumeier J J, Tesmer J, Thompson J D and Wu X D 1995 *Appl. Phys. Lett.* **67** 860
[93] Dörr K, Müller K-H, Kozlova N, Reutler P, Klingeler R, Büchner B and Schultz L 2005 *J. Magn. Magn. Mater.* **290–291** 416
[94] Salamon M B and Jaime M 2001 *Rev. Mod. Phys.* **73** 583
[95] Millis A J, Mueller R and Boris I Shraiman 1996 *Phys. Rev.* B **54** 5389
[96] Millis A J, Shraiman R and Mueller R 1996 *Phys. Rev. Lett.* **77** 175
[97] Burgy J, Moreo A and Dagotto E 2004 *Phys. Rev. Lett.* **92** 097202
[98] Mayr M, Moreo A, Vergés J A, Arispe J, Feiguin A and Dagotto E 2001 *Phys. Rev. Lett.* **86** 135
[99] Murakami S and Nagaosa N 2003 *Phys. Rev. Lett.* **90** 197201
[100] Mathieu R, Akahoshi D, Asamitsu A, Tomioka Y and Tokura Y 2004 *Phys. Rev. Lett.* **93** 227202
[101] Haghiri-Gosnet A-M and Renard J-P 2003 *J. Phys. D: Appl. Phys.* **36** R127
[102] Prellier W, Lecoeur Ph and Mercey B 2001 *J. Phys. Cond. Matt.* **13** R915
[103] Prellier W, Singh M P and Murugavel P 2005 *J. Phys. Cond. Matt.* **17** R803
[104] Joshi S, Nawathey R, Koinkar V N, Godbole V P, Chaudhari S M, Ogale S B and Date S K 1988 *J. Appl. Phys* **64** 5647
[105] Holzapfel B, Roas B, Schultz L, Bauer P and Saemann-Ischenko G 1992 *Appl. Phys. Lett.* **61** 3178
[106] Chahara K, Ohno T, Kasai M and Kozono Y 1993 *Appl. Phys. Lett.* **63** 1990
[107] Jin S, Tiefel T H, McCormack M, Fastnacht R A, Ramesh R and Chen L H 1994 *Science* **264** 413
[108] Li K, Qi Z, Li X, Zhu J and Zhang Y 1997 *Thin Solid Films* **304** 386
[109] Vlakhov E S, Chakalov R A, Chakalova R I, Nenkov K A, Dörr K, Handstein A and Müller K-H 1998 *J. Appl. Phys.* **83** 2152
[110] Kawasaki M, Izumi M, Konishi Y, Manako T and Tokura Y 1999 *Mater. Sci. Eng.* B **63** 49–57
[111] Venkatesan T, Wu X D, Dutta B, Inam A, Hegde M S, Hwang D M, Chang C C, Nazar L and Wilkens B 1989 *Appl. Phys. Lett.* **54** 581
[112] Jo M-H, Mathur N D, Evetts J E and Blamire M G 1999 *Appl. Phys. Lett.* **75** 3689
[113] Tanaka H, Kawai T 2000 *Appl. Phys. Lett.* **76** 3618
[114] Klein J, Höfener C, Alff L and Gross R 2000 *J. Magn. Magn. Mater.* **211** 9

[115] Mercey B, Salvador P A, Lecoeur P, Prellier W, Hervieu M, Simon C, Chippaux D, Haghiri-Gosnet A M and Raveau B 2003 *J. Appl. Phys.* **94** 2716

[116] Rosina M, Audier M, Dubourdieu C, Frohlich K and Weiss F 2003 *J. Cryst. Growth* **259** 358

[117] Venkataiah G, Krishna D C, Vithal M, Rao S S, Bhat S V, Pradas V, Subramanyam and Venugopal Reddy P 2005 *Physica* B **357** 370

[118] Moshnyaga A, Khoroshun I, Sidorenko A and Petrenko P 1999 *Appl. Phys. Lett.* **74** 2842

[119] Walter T, Dörr K, Müller K-H, Holzapfel B, Eckert D, Wolf M, Schläfer D, Schultz L and Grötzschel R 1999 *Appl. Phys. Lett.* **74** 2218

[120] Ziese M, Semmelhack H C, Han K H, Sena S P and Blythe H J 2002 *J. Appl. Phys.* **91** 9930

[121] Thiele C, Dörr K, Schultz L, Meyer D C, Levin A A, Fähler S and Paufler P 2005 *Appl. Phys. Lett.* **87** 262502

[122] Kim J-H, Khartsev S I and Grishin A M 2003 *Appl. Phys. Lett.* **82** 4295

[123] Yoo Y-Z, Ahmet P, Jin Z-W, Nakajima K, Chikyow T, Kawasaki M, Konishi Y, Yonezawa Y, Song J H and Koinuma H 2003 *Appl. Phys. Lett.* **82** 4125

[124] McKee R A, Walker F J and Chisholm M F 1998 *Phys. Rev. Lett.* **81** 3014

[125] Rijnders G, Koster G, Blank D H A and Rogalla H 1997 *Appl. Phys. Lett.* **70** 1888

[126] Rijnders G, Blank D H A, Choi J and Eom C B 2004 *Appl. Phys. Lett.* **84** 505

[127] Koster G, Rjinders G J H M, Blank D H A and Rogalla H 1999 *Appl. Phys. Lett.* **74** 3729

[128] Dörr K, De Teresa J M, Müller K-H, Eckert D, Walter T, Vlakhov E, Nenkov K and Schultz L 2000 *J. Phys.: Condens. Matter* **12** 7099

[129] Lu Y, Li X W, Gong G Q, Xiao G, Grupta A, Lecoeur P, Sun J Z, Wang Y Y and Dravid V P 1996 *Phys. Rev.* B **54** 8357

[130] Gupta A and Sun J Z 1999 *J. Magn. Magn. Mater.* **200** 24

[131] Sahana M, Walter T, Dörr K, Müller K-H, Eckert D and Brand K 2001 *J. Appl. Phys.* **89** 6834

[132] Salvador P A, Haghiri-Gosnet A-M, Mercey B, Hervieu M and Raveau B 1999 *Appl. Phys. Lett.* **75** 2638

[133] Luo Y, Käufler A and Samwer K 2000 *Appl. Phys. Lett.* **77** 1508

[134] Silly F and Castell M R 2005 *Phys. Rev. Lett.* **94** 046103

[135] Worledge D C and Geballe T H 2000 *Appl. Phys. Lett.* **76** 900

[136] Thiele C, Dörr K, Schultz L, Beyreuther E and Lin W-M 2005 *Appl. Phys. Lett.* **87** 162512

[137] Céspedes O, Watts S M, Coey J M D, Dörr K and Ziese M 2005 *Appl. Phys. Lett.* **87** 083102

[138] Gommert E, Cerva H, Wecker J and Samwer K 1999 *J. Appl. Phys.* **85** 5417

[139] Maurice J-L, Pailloux F, Barthélémy A, Durand O, Imhoff D, Lyonnet R, Rocher A and Contour J-P 2003 *Phil. Mag.* **83** 3201

[140] Liang Y C, Wu T B, Lee H Y and Liu H J 2004 *Thin Solid Films* **469–470** 500

[141] Yang Z Q, Hendrikx R, Aarts J, Qin Y L, Zandbergen H W 2004 *Phys. Rev.* B **70** 174111

[142] Wiedenhorst B, Höfener C, Lu Y, Klein J, Alff L, Gross R, Freitag B H, Mader W 1999 *Appl. Phys. Lett.* **74** 3636

[143] Lebedev O I, Tendeloo G V, Amelinckx S, Leibold B and Habermeier H-U 1998 *Phys. Rev.* B **58** 8065

[144] Pailloux F, Imhoff D, Sikora T, Barthélémy A, Maurice J-L, Contour J-P, Colliex C and Fert A 2002 *Phys. Rev.* B **66** 014417

[145] Samet L, Imhoff D, Maurice J-L, Contour J-P, Gloter A, Manoubi T, Fert A and Colliex C 2003 *Eur. Phys. J.* B **34** 179–92

[146] Akiyama R, Tanaka H, Matsumoto T and Kawai T 2001 *Appl. Phys. Lett.* **79** 4378

[147] Grévin B, Maggio-Aprile I, Bentzen A, Kuffer O, Joumard I and Fischer Ø 2002 *Appl. Phys. Lett.* **80** 3979

[148] Paranjape M, Raychaudhuri A K, Mathur N D and Blamire M G 2003 *Phys. Rev.* B **67** 214415

[149] Wu Y, Suzuki Y, Rüdiger U, Yu J, Kent A D, Nath T K and Eom C B 1999 *Appl. Phys. Lett.* **75** 2295

[150] Soh Y-A, Aeppli G, Mathur N D and Blamire M G 2000 *Phys. Rev.* B **63** 020402

[151] Soh Y-A, Evans P G, Cai Z, Lai B, Kim C-Y, Aeppli G, Mathur N D, Blamire M G and Isaacs E D 2002 *Appl. Phys. Lett.* **91** 7742

[152] Soh Y-A, Aeppli G, Kim C-Y, Mathur N D and Blamire M G 2003 *J. Appl. Phys.* **93** 8322

[153] Popov G, Kalinin S V, Alvarez T, Emge T J, Greenblatt M, Bonnell D A 2002 *Phys. Rev.* B **65** 064426

[154] Jung G, Markovich V, Mogilyanski D, van der Beek C, Mukovskii Y M 2005 *J. Magn. Magn. Mater.* **290–291** 902

[155] Tokunaga M, Tokunaga Y and Tamegai T 2004 *Phys. Rev. Lett.* **93** 037203

[156] Sukhorukov Yu P, Gan'shina E A, Belevtsev B I, Loshkareva N N, Vinogradov A N, Rathnayaka K D D, Parasiris A and Naugle D G 2002 *J. Appl. Phys.* **91** 4403

[157] Vlasko-Vlasov V K, Lin Y, Welp U, Crabtree G W, Miller D J and Nikitenko V I 2000 *J. Appl. Phys.* **87** 5828

[158] Rauer R, Neuber G, Kunze J, Bäckström J, Rübhausen M, Walter T, Dörr K 2004 *J. Magn. Magn. Mater.* **290–291** 948

[159] Kirilyuk A 2002 *J. Phys. D: Appl. Phys.* **35** R189

[160] Fiebig M, Pavlov V V and Pisarev R V 2005 *J. Opt. Soc. Am.* B **22** 96

[161] McGill S A, Miller R I, Torrens O N, Mamchik A, Chen I-W and Kikkawa J M 2004 *Phys. Rev. Lett.* **93** 047402

[162] Fiebig M 2005 *J. Phys. D: Appl. Phys.* **38** R123

[163] McIlroy D N, Waldfried C, Zhang J, Choi J-W, Foong F, Liou S H and Dowben P A 1996 *Phys. Rev.* B **54** 17438

[164] Choi J, Zhang J, Jiou S-H, Dowben P A and Plummer E W 1999 *Phys. Rev.* B **59** 13453

[165] de Jong M P, Dediu V A, Taliani C and Salaneck W R 2003 *J. Appl. Phys.* **94** 7292

[166] Borca C N, Ristoiu D, Xu Q L, Liou S-H, Adenwalla S and Dowben P A 2000 *J. Appl. Phys.* **87** 6104

[167] Beyreuther E, Eng L, Thiele C, Dörr K and Grafström S 2006 *Phys. Rev.* B at press

[168] Park J-H, Vescovo E, Kim H-J, Kwon C, Ramesh R and Venkatesan T 1998 *Phys. Rev. Lett.* **81** 1953

[169] Park J H, Vescovo E, Kim H J, Kwon C, Ramesh R and Venkatesan T 1998 *Nature* **392** 794

[170] Aarts J, Freisem S, Hendrikx R and Zandbergen H W 1998 *Appl. Phys. Lett.* **72** 2975

[171] Praus R B, Leibold B, Gross G M and Habermeier H-U 1999 *Appl. Sur. Sci.* **138–139** 40

[172] Walter T, Dörr K, Müller K H, Eckert D, Nenkov K, Hecker M, Lehmann M and Schultz L 2000 *J. Magn. Magn. Mater.* **222** 175

[173] Sun J Z, Abraham D W, Rao R A and Eom C B 1999 *Appl. Phys. Lett.* **74** 3017

[174] Bibes M, Balcells Ll, Valencia S, Fontcuberta J, Wojcik M, Jedryka E and Nadolski S 2001 *Phys. Rev. Lett.* **87** 067210

[175] Walter T 2004 *PhD thesis* University of Technology, Dresden, Germany

[176] Ju H L and Krishnan K M 1998 *J. Appl. Phys.* **83** 7073

[177] Zhang J, Tanaka H, Kanki T, Choi J H and Kawai T 2001 *Phys. Rev.* B **64** 184404

[178] Millis A J, Darling T and Migliori A 1998 *J. Appl. Phys.* **83** 1588

[179] Chen X J, Soltan S, Zhang H and Habermeier H-U 2002 *Phys. Rev.* B **65** 174402

[180] Klein J, Philipp J B, Carbone G, Vigliante A, Alff L and Gross R 2001 *Phys. Rev.* B **66** 052414

[181] Suzuki Y, Hwang H Y, Cheong S-W and van Dover R B 1997 *Appl. Phys. Lett.* **71** 140

[182] Nath T K, Rao R A, Lavric D, Eom C B, Wu L and Tsui F 1999 *Appl. Phys. Lett.* **74** 1615
[183] Steenbeck K and Hiergeist R 1999 *Appl. Phys. Lett.* **75** 1778
[184] Wu X W, Rzchowski M S, Wang H S and Qi Li 2000 *Phys. Rev.* B **61** 501
[185] Rauer R, Bäckström J, Budelmann D, Kurfiß M, Schilling M, Rübhausen M, Walter T, Dörr K and Cooper S L 2002 *Appl. Phys. Lett.* **81** 3777
[186] Kozlova N, Walter T, Dörr K, Eckert D, Handstein A, Skourski Y, Müller K H and Schultz L 2004 *Physica* B **346–347** 74
[187] Hwang H Y, Cheong S W, Ong N P and Batlogg B 1996 *Phys. Rev. Lett.* **77** 2041
[188] Helman J S and Abeles B 1976 *Phys. Rev. Lett.* **37** 1429
[189] Steenbeck K, Eick T, Kirsch K, O'Donnell K and Steinbeiß 1997 *Appl. Phys. Lett.* **71** 968
[190] Evetts J E, Blamire M G, Mathur N D, Isaac S P, Teo B-S, Cohen L F and Macmanus-Discroll J L 1998 *Phil. Trans. R. Soc. Lond.* A **356** 1593
[191] Klein J , Höfener C , Uhlenbruck S , Alff L , Büchner B and Gross R 1999 *Europhys. Lett.* **47** 371
[192] Gross R *et al* 2000 *J. Magn. Magn. Mat.* **211** 150
[193] Gunnarsson R, Kadigrobov A and Ivanov Z 2002 *Phys. Rev.* B **66** 024404
[194] Schiffer P, Ramirez A P, Bao W and Cheong S-W 1995 *Phys. Rev. Lett.* **75** 3336
[195] Balcells l, Fontcuberta J, Martínez B and Obradors X 1998 *Phys. Rev.* B **58** R14697
[196] Ziese M, Heydon G, Höhne R, Esquinazi P and Dienelt J 1999 *Appl. Phys. Lett.* **74** 1481
[197] Lee S, Hwang H Y, Boris I Shraiman, Ratcliff II W D and Cheong S-W 1999 *Phys. Rev. Lett.* **82** 4508
[198] Paranjape M, Mitra J, Raychaudhuri A K, Todd N K, Mathur N D and Blamire M G 2003 *Phys. Rev.* B **68** 144409
[199] Simmons J G 1962 *J. Appl. Phys.* **34** 238
[200] Simmons J G and Unterkofler G J 1962 *J. Appl. Phys.* **34** 1828
[201] Glazman L I and Matveev K A 1988 *Sov. Phys. JETP* **67** 1276
[202] Furukawa N 1997 *J. Phys. S. Japan* **66** 2523
[203] Guinea F 1998 *Phys. Rev.* B **58** 9212
[204] Inoue J and Maekawa S 1996 *Phys. Rev.* B **53** R11927
[205] Ziese M, Bollero A, Panagiotopoulos and Moutis N 2005 *Phys. Rev.* B **72** 024453
[206] Sun H, Yu K W and Li Z Y 2003 *Phys. Rev.* B **68** 054413
[207] Bowen M, Bibes M, Barthélémy A, Contour J-P, Anane A, Lemaître Y and Fert A 2003 *Appl. Phys. Lett.* **82** 233
[208] O'Donnell J, Andrus A E, Oh S, Colla E V and Eckstein J N 2000 *Appl. Phys. Lett.* **76** 1914
[209] Jo M-H, Mathur N D, Evetts J E and Blamire M G 2000 *Appl. Phys. Lett.* **77** 3803
[210] Jo M-H, Mathur N D, Todd N K and Blamire M G 2000 *Phys. Rev.* B **61** 14905
[211] Jo M-H, Blamire M G, Ozkaya D and Petford-Long A K 2003 *J. Phys.: Condens. Matter* **15** 5243
[212] Bibes M, Bowen M, Barthélémy A, Anane A, Bouzehouane K, Carrétéro C, Jacquet E, Contour J-P and Durand O 2003 *Appl. Phys. Lett.* **82** 3269
[213] De Teresa J M, Barthélémy A, Fert A, Contour J P, Lyonnet R, Montaigne F and Seneor P 1999 *Science* **286** 507
[214] De Teresa J M, Barthélémy A, Fert A, Contour J P, Lyonnet R, Montaigne F, Seneor P and Vaurés A 1999 *Phys. Rev. Lett.* **82** 4288
[215] Sun J Z, Roche K P and Parkin S S P 2000 *Phys. Rev.* B **61** 11244
[216] Worledge D C and Geballe T H 2000 *Phys. Rev. Lett.* **85** 5182
[217] Hu G and Suzuki Y 2002 *Phys. Rev. Lett.* **89** 276601
[218] Baszyński J, Toliński T 2000 *Acta Phys. Pol.* A **98** 567
[219] Versluijs J J, Bari M A and Coey J M D 2001 *Phys. Rev. Lett.* **87** 026601
[220] Tedrow P M and Meservey R 1971 *Phys. Rev. Lett.* **26** 192
[221] Tedrow P M and Meservey R 1971 *Phys. Rev. Lett.* **24** 1004
[222] Meservey R and Tedrow P M 1994 *Phys. Rep.* **238** 173
[223] Sharma M, Wang S X and Nickel J H 1999 *Phys. Rev. Lett.* **82** 616
[224] Ukraintsev V A 1996 *Phys. Rev.* B **53** 11176
[225] Jo M-H, Mathur N D and Blamire M G 2002 *Appl. Phys. Lett.* **80** 2722
[226] Myers E B, Ralph D C, Katine J A, Louie R N and Buhrman R A 1999 *Science* **285** 867
[227] Gilabert A *et al* 2001 *Appl. Phys. Lett.* **78** 1712
[228] Garcia V, Bibes M, Barthélémy A, Bowen M, Jacquet E, Contour J-P and Fert A 2004 *Phys. Rev.* B **69** 052403
[229] Yuasa S, Nagahama T, Fukushima A, Suzuki Y and Ando K 2004 *Nature Mater.* **3** 868
[230] McNally F, Kim J H and Lange F F 2000 *J. Mater. Res.* **15** 1546
[231] Hill N A and Filippetti A 2001 *J. Magn. Magn. Mater.* **242** 976
[232] Hill N A 2000 *J. Phys. Chem.* B **104** 6694
[233] Lottermoser T, Lonkai T, Amann U, Hohlwein D, Ihringer J and Fiebig M 2004 *Nature* **430** 541
[234] Kimura T, Goto T, Shintani H, Ishizaka K, Arima T and Tokura Y 2003 *Nature* **426** 55
[235] Goto T, Kimura T, Lawes G, Ramirez A P and Tokura Y 2004 *Phys. Rev. Lett.* **92** 257201
[236] Hur N, Park S, Sharma P A, Guha S and Cheong S-W 2004 *Phys. Rev. Lett.* **93** 107207
[237] Hur N, Park S, Shama P A, Ahn J S, Guha S and Cheong S W 2004 *Nature* **429** 392
[238] Kimura T, Kawamoto S, Yamada I, Azuma M, Takano M and Tokura Y 2003 *Phys. Rev.* B. **67** 180401
[239] Hemberger J, Lunkenheimer P, Fichtl R, Krug von Nidda H-A, Tsurkan V and Loidl A 2005 *Nature* **434** 364
[240] Terai K, Ohnishi T, Lippmaa M, Koinuma H and Kawasaki M 2004 *Japan. J. Appl. Phys.* **43** L227
[241] Laletsin U, Padubnaya N, Srinivasan G and Devreugd C P 2004 *Appl. Phys.* A **78** 33
[242] Srinivasan G, Rasmussen E T and Hayes R 2003 *Phys. Rev.* B **67** 014418
[243] Shastry S, Srinivasan G, Bichurin M I, Petrov V M and Tatarenko A S 2004 *Phys. Rev.* B **70** 064416
[244] Ahn C H, Triscono J-M and Mannhart J 2003 *Nature* **424** 1015
[245] Ogale S B, Talyansky V, Chen C H, Ramesh R, Greene R L and Venkatesan T 1996 *Phys. Rev. Lett.* **77** 1159
[246] Mathews S, Ramesh R, Venkatesan T and Benedetto J 1997 *Science* **276** 238
[247] Tabata H and Kawai T 1997 *IEICE Trans. Electron.* **E80**-C 918
[248] Wu T, Ogale S B, Garrison J E, Nagaraj B, Biswas A, Chen Z, Greene R L, Ramesh R, Venkatesan T and Millis A J 2001 *Phys. Rev. Lett.* **86** 5998
[249] Hong X , Posadas A, Lin A and Ahn C H 2003 *Phys. Rev. Lett.* **68** 134415
[250] Kanki T, Park Y G, Tanaka H and Kawai T 2003 *Appl. Phys. Lett.* **83** 4860
[251] Zhao T, Ogale S B, Shinde S R and Ramesh R 2004 *Appl. Phys. Lett.* **84** 750
[252] Eblen-Zayas M, Bhattacharya A, Staley N E, Kobinskii A L and Goldman A M 2005 *Phys. Rev. Lett.* **94** 037204
[253] Lee M K, Nath T K, Eom C B, Smoak M C and Tsui F 2000 *Appl. Phys. Lett.* **77** 3547
[254] Dale D, Fleet A, Brock J D and Suzuki Y 2003 *Appl. Phys. Lett.* **82** 3725
[255] Zheng H *et al* 2004 *Science* **303** 661
[256] Park S-E and Shrout T R 1997 *J. Appl. Phys.* **82** 1804
[257] Kim Y N, Chi E O, Kim J C, Lee E K and Hur N H 2003 *Solid State Commun.* **128** 339